

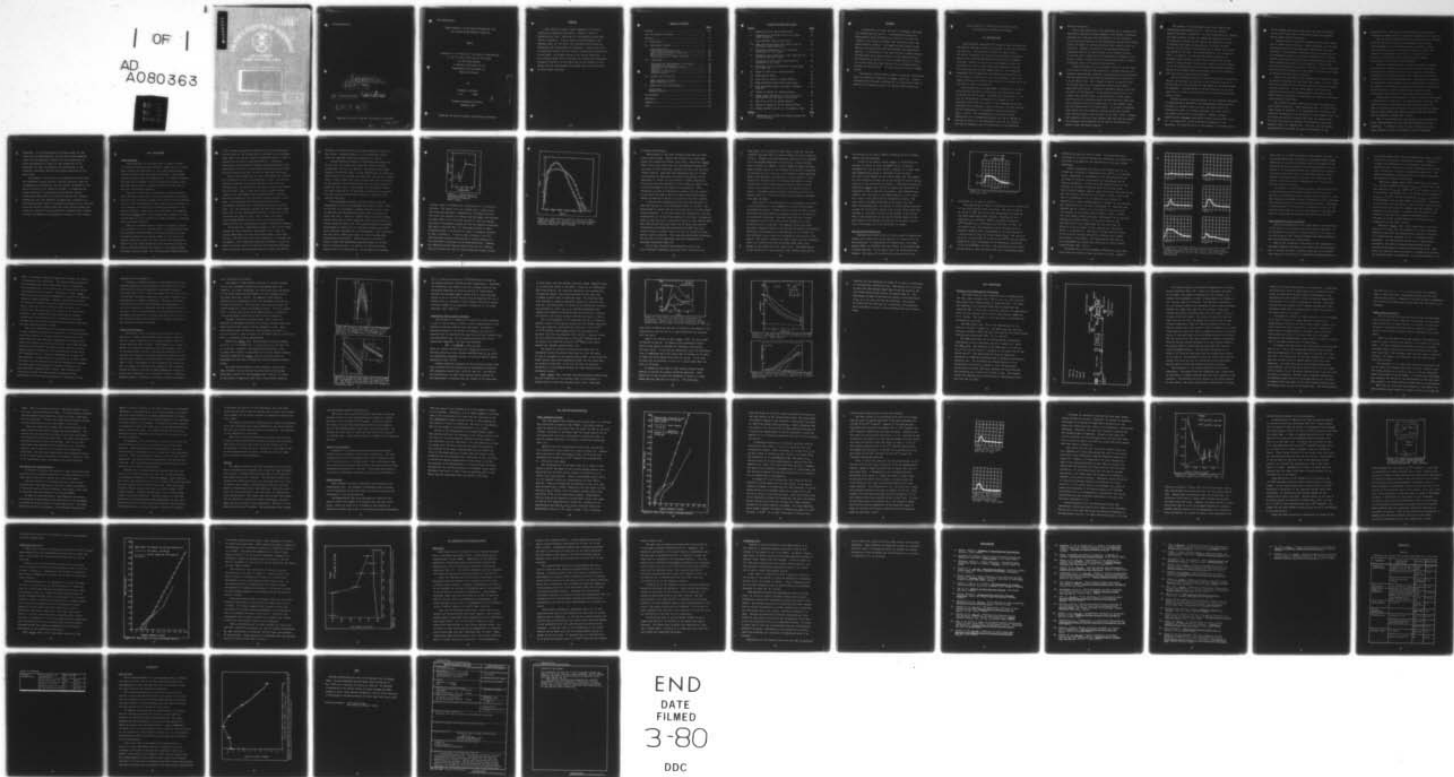
AD-A080 363

AIR FORCE INST OF TECH WRIGHT-PATTERSON AFB OH SCHOO--ETC F/6 20/12
LASER ANNEALING OF AND LASER INTERACTIONS WITH ION IMPLANT SEMI--ETC(U)
DEC 79 K R BRADLEY
AFIT/6EP/PH/79D-1

UNCLASSIFIED

NL

| OF |
AD
A080363



AFIT/GEP/PH/79D-1

6 LASER ANNEALING OF
AND LASER INTERACTIONS WITH
ION IMPLANT SEMICONDUCTING MATERIALS.

9 Master's THESIS,

14 AFIT/GEP/PH/79D-1

10 KENNETH R. BRADLEY
2 Lt USAF

DDC
RECEIVED
FEB 7 1980
REGISTERED
A

11 Dec 79

12 74

Approved for public release; distribution unlimited

80

2

5

147

012 225

AFIT/GEP/PH/79D-1

LASER ANNEALING OF AND LASER INTERACTIONS WITH
ION IMPLANT SEMICONDUCTING MATERIALS

THESIS

Presented to the Faculty of the School of Engineering
of the Air Force Institute of Technology
Air Training Command
in Partial Fulfillment of the
Requirements for the Degree of
Master of Science

by

Kenneth R. Bradley
2 Lt. USAF

Graduate Engineering Physics
December 1979

| | |
|--------------------|-------------------------------------|
| Accession For | |
| DTIC TAB | <input checked="" type="checkbox"/> |
| Unannounced | <input type="checkbox"/> |
| Justification | |
| Distribution/ | |
| Availability Codes | |
| Dist | Avail and/or special |
| A | |

Approved for public release; distribution unlimited

PREFACE

I have found the work in laser annealing to be both a learning and rewarding experience. Although I did not accomplish all that I had hoped to, the results do show some useful information. I would like to thank my advisor, Dr. Theodore Luke, for the advice and counseling which made the experiment both interesting and rewarding. I would also like to thank Bill Mullins for the optical reflectivity measurements he performed. My thanks also go to Dr. Robert Hengehold, Maj. Michael Stamm, and Dr. Won Roh for the help they provided. My special thanks go to my wife Kathy for the typing of this paper, and the understanding she showed which made completion of this project possible.

TABLE OF CONTENTS

| | <u>Page</u> |
|--|-------------|
| Preface | iii |
| List of Figures and Tables | v |
| Abstract | iv |
| I. INTRODUCTION | 1 |
| II. BACKGROUND MATERIAL | 7 |
| Laser Annealing | 7 |
| Time-Resolved Reflectivity | 14 |
| Laser Absorption During Annealing. | 18 |
| Plasma Surface Damage | 21 |
| Theoretical Work on Laser Annealing | 24 |
| III. EXPERIMENT | 29 |
| Equipment and Experimental Arrangement | 29 |
| Experimental Procedures | 33 |
| Calibration and Reproducibility. | 34 |
| Samples | 36 |
| Analysis of Annealing | 37 |
| Error Analysis | 37 |
| IV. RESULTS AND DISCUSSION | 39 |
| Laser Annealing of GaAs | 39 |
| Laser Annealing of Si | 48 |
| V. CONCLUSIONS AND RECOMMENDATIONS | 52 |
| Conclusions | 52 |
| Recommendations | 55 |
| Bibliography | 57 |
| Appendix A | 61 |
| Appendix B | 63 |
| Vita | 65 |

LIST OF FIGURES AND TABLES

| <u>Figure</u> | | <u>Page</u> |
|---------------|---|-------------|
| 1 | Reflectivity vs. argon laser power | 10 |
| 2 | Concentration profiles of As in Si after laser annealing | 11 |
| 3 | Time-resolved reflectivity trace | 15 |
| 4-9 | HeNe reflected signal from virgin GaAs at different energy densities | 17 |
| 10 | Frequency dependences of the breakdown thresholds of inert gases | 23 |
| 11 | Threshold power densities in the breakdown of molecular and inert gases | 23 |
| 12 | Calculated surface layer temperature of amorphous Si vs. time | 26 |
| 13 | Predicted position dependence of temperature for virgin Si | 27 |
| 14 | Depth of melting vs. energy density | 27 |
| 15 | Experimental setup | 30 |
| 16 | Melt time of GaAs vs. energy density | 40 |
| 17 | HeNe reflected signal from virgin GaAs | 43 |
| 18 | HeNe reflected signal from GaAs implanted with Te | 43 |
| 19 | Degree of damage vs. energy density | 45 |
| 20 | Laser energy dependence of the extinction coefficient and the sheet resistivity | 47 |
| 21 | Melt time of Si vs. energy density | 49 |
| 22 | Degree of damage in Si vs. energy density | 51 |
| 23 | Energy density profile of the annealing beam | 64 |
| <u>Tables</u> | | <u>Page</u> |
| I | References to thermal and optical properties of Si and GaAs | 61 |

ABSTRACT

A Q-switched ruby laser was used to irradiate implanted and unimplanted GaAs and Si. Time-resolved reflectivity measurements, which determine the length of time that the surface of the sample is melted, were performed during the laser annealing process. The length of melt versus energy density was plotted for both the implanted and unimplanted samples. No difference in the melt time was observed between implanted and unimplanted samples at high energy densities. The threshold for melting in the implanted samples was found to be lower than the virgin samples, and the energy density required to produce melting in GaAs was about 2/5 that needed for Si.

The results obtained were compared to reported experimental work and numerical calculation on laser annealing. Optical reflectivity techniques, performed by Lt. Mullins were used to determine the crystallinity of the samples after annealing.

LASER ANNEALING OF AND LASER INTERACTIONS WITH ION IMPLANT SEMICONDUCTING MATERIALS

I. INTRODUCTION

Semiconducting materials like Germanium (Ge), Silicon (Si), and Gallium Arsenide (GaAs) are important to both the Air Force and industry. Semiconducting material is used to make electrical components for devices such as optical detectors, solar cells, and microelectronic circuits such as computer memories. Optical components such as windows, lenses, and modulators can also be made using semiconducting material. The semiconducting material used in many of the electrical components must be doped with an impurity to form either an n-type layer, a p-type layer, or a p-n junction. One of the newest techniques for making these layers or junctions is by ion implantation (Ref. 1,2,3, and 4).

Ion implantation is accomplished by bombarding a piece of semiconducting material or substrate, such as silicon, with a certain type of impurity. The depth and distribution of the ions in the substrate is related to the energy of the bombarding ions (Ref. 2,3, and 5). The concentration of the implanted ions is related to the ion current, the time exposed, and the temperature of the substrate during implantation (Ref. 5 and 6). The concentration, the depth, and the distribution of the implanted material can now be changed by varying the energy of the bombarding ions, the ion current, the time of exposure, and the temperature of the substrate

during implantation.

One of the objectives of ion implantation is to increase the electrical conductivity which depends on the number of carriers available for conduction and the mobility of the electrons. If the impurity atoms can be substitutionally placed into lattice sites, the number of carriers available for conduction will be increased. However, the mobility is decreased during ion implantation because it causes damage to the crystal lattice. To increase the conductivity it is important the damage to the crystal lattice be small and that the impurity atoms be substitutionally placed into crystal lattice sites.

Another objective for ion implanted materials is that they can be used in infrared (IR) detectors. In both extrinsic and intrinsic semiconductor crystals, the valence band and conduction band are separated by the band gap energy which in silicon is 1.12 eV (Ref. 7:54). For a photon to excite an electron from the valence band into the conduction band it would need at least that much energy. Therefore, extrinsic silicon would not be useful in IR detectors. In an extrinsic semiconductor or a crystal with impurity atoms in substitutional lattice sites there is also an ionization energy between the donor level and the conduction band of an n-type layer, or the acceptor level and the valence band of a p-type layer. In p-type Si implanted with indium (In) the ionization energy between the acceptor level and the valence band is about .16 eV (Ref. 7:63). Because the ionization energy is much smaller than the band gap energy, the extrinsic semiconductors can be used in IR detectors to detect longer wavelength photons.

The process of ion implantation has both benefits and disadvantages associated with it. Some of the reported benefits are (Ref. 3,6,and 8): (1) the concentration of dopants for laser annealed samples can exceed the solubility limit, (2) masking of either the ion beam or the sample can be done to produce many doping configurations, (3) known impurity dopant, and (4) depth of the dopants can be varied by changing the energy of the ions. The disadvantages of the process are (Ref. 2, 6,and 9): (1) the impurity atoms bombarding the substrate cause disorder in the crystal lattice such as dislocation loops, stacking faults, and clusters of point defects, (2) at high concentrations of impurity atoms complete amorphization of the crystal lattice is caused, and (3) ions seldom go into the lattice sites substitutionally.

For the implanted material to have the electrical properties desired in the layers or junctions, the impurities need to be substituted into the lattice, and the damage to the lattice must be repaired. A process known as thermal annealing is the most common way to repair the lattice and to get the impurities into lattice sites.

Thermal annealing involves heating of the implanted substrate to temperatures of 800-900° C for approximately thirty minutes. Although the substrate does not melt, the atoms within the substrate are able to re-order themselves and repair much of the damage caused by ion implantation. However, thermal annealing also has some undesirable effects such as (Ref. 2 and 9): (1) degradation of the electrical properties of the substrate, (2) redistribution of the dopants, (3) contamination

of the surface with other impurities, (4) drop in minority carrier life time, and (5) dislocation loops and stacking faults resist thermal annealing.

Another method of annealing involves using a laser beam, and is called laser annealing. Pulsed neodymium, pulsed ruby, and cw-argon are the most frequently used lasers for laser annealing. The mechanism responsible for laser annealing is not entirely understood but there is evidence that for nano-second pulsed laser annealing the material actually melts and then recrystallizes (Ref. 10,11,12,and 13). For cw laser annealing the process appears to be similar to thermal annealing but the time of heating due to the laser is less than that used in thermal annealing (Ref. 10 and 13).

Credit for discovering laser annealing is given to a group of Russian scientists who published their report in 1974. Since that time, scientists all over the world have shown an interest in laser annealing. In the United States the most active scientific groups are Bell Laboratories in New Jersey, Oak Ridge National Laboratory in Tennessee, and Stanford Electronics Laboratories in California.

The interest in laser annealing is due to its advantages over thermal annealing. These advantages are: (1) most of the laser energy is absorbed in the implanted area; therefore, the electrical properties of the substrate are not affected (Ref. 14), (2) since the process is rapid, the amount of contamination from the environment is reduced, (3) dislocation loops and stacking faults are removed (Ref. 3 and 14), (4) the carrier concentrations can exceed the limit of solubility of the

impurities (Ref. 9:227), and (5) the process is fast and no furnaces are needed making it ideal for industry (Ref. 2 and 3).

Most of the published papers deal with work done on silicon. There has also been some work on Germanium (Ge), Gallium Arsenide (GaAs), and other semiconducting materials. These reports usually examine the observed changes in either the physical or electrical properties of the substrate as a function of either the laser annealing energy density (joules/cm²) or the power density (MW/cm²).

In many of these reports, two specific values are given: (1) annealing threshold, and (2) critical damage threshold. Although these quantities are not well defined, they usually correspond to a specific change in the physical or electrical properties of the implanted substrate. The annealing threshold is usually the lowest energy or power density where a change in the physical or electrical properties is observed. The critical damage threshold is where visual damage such as craters, microcracks, and cavities in the surface begin to appear.

Visual damage is the easiest to detect; however, other types of damage such as decrease in photoconductivity, mobility, and carrier density can be caused by laser annealing (Ref. 4). Lack of consensus exists regarding how the laser flux or energy density causes damage but several attempts have been made to find an acceptable theory (Ref. 15:37).

Most of the theoretical work has dealt not only with the laser induced damage but also with the mechanisms of laser annealing. A universal theory is very difficult since the laser annealing process is dependent upon the following

variables: (1) the wavelength of the laser used, (2) the laser flux or energy density, (3) the time of the annealing pulse, (4) the substrate material, (5) the temperature in which the annealing is done, (6) the orientation of the substrate, (7) the concentration and distribution of the implanted impurities, and (8) the spatial uniformity of the laser flux.

The purpose of this thesis is to examine the effect that the wavelength, energy density, substrate material, type and concentration of impurities, and the spatial uniformity of the laser flux have on the annealing process. By comparing the results obtained by time-resolved reflectivity, optical reflectivity (Ref. 22), and visible microscopy with reported experimental work and numerical calculations, information on how these variables affect the annealing process will be obtained. Also, one proposed theory states that laser induced damage may be due to a plasma at the air-substrate interface (Ref. 16:637); this will be examined to determine the validity of this theory.

II. BACKGROUND

Laser Annealing

Laser annealing is one method that is used to anneal ion implanted semiconducting material. Annealing is a process which assists the implanted ions to occupy substitutional crystal lattice sites, and repair the damage in the crystal lattices caused by the ion implantation. For thermal annealing, the heat from a furnace is used to anneal the samples, while for laser annealing the irradiation from the laser beam is used for the annealing process.

Since the first paper was published on laser annealing there has been a great deal of laser annealing work performed. The term laser annealing; however, has not been clearly defined. In most of the published work laser annealing is considered to occur whenever the physical or electrical properties of the material undergo a change that can be detected. For example, Khaibullin, et.al. (Ref. 9:225) define laser annealing to have occurred when the laser irradiation causes electrical activation of an implanted impurity.

Some of the methods used to examine the physical changes in the samples are: (1) visible (Ref. 5), electron (Ref.9 and 14), and phase contrast (Ref. 10) microscopy which are used to examine changes in the surface layer of the sample, (2) optical reflectance (Ref. 10,11,17, and 18) and transmission (Ref.11) of the sample during the laser annealing process are used to determine whether the surface of the sample melted, (3) Raman Scattering (Ref. 19), (4) Rutherford backscattering

which is used to examine the impurities not in substitutional lattice sites of the crystal (Ref. 12,19,and 20), (5) ellipsometry (Ref. 21), and (6) optical reflectivity which is used to examine the crystalline structure (Ref.22). Electrical measurements which determine whether the impurities have been electrically activated such as sheet resistivity (Ref.9 and21) and Hall measurements (Ref. 14 and 23) have been performed.

During laser annealing, the laser irradiation is absorbed by the material causing its temperature to rise. As the temperature increases, the atomic mobility of the atoms will increase making it possible for the atoms to move into crystal lattice sites. Heat is then dissipated by either thermal conduction or reradiated from the surface (Ref. 3 and 24). The exact mechanism of the annealing process; however, is not known. Two mechanisms that have been identified are a solid-phase epitaxial and a liquid-phase epitaxial regrowth (Ref. 13). The difference between the solid and liquid phase being that for the liquid-phase epitaxial regrowth the entire implanted area needs to melt. Due to their high energy output pulsed Nd:YAG and ruby lasers are the most common lasers used for the liquid-phase epitaxial regrowth experiments.

The process for liquid-phase epitaxy is that as the sample absorbs the laser energy its temperature rises. Once the surface temperature is above the melting point it will begin to melt. The melt front will then continue to move deeper into the sample. For liquid-phase epitaxial regrowth to occur the depth of the melt must be as deep as the implanted impurities. After the energy absorbed drops below the energy lost by the

material, the melted front will recede toward the surface of the sample. Recrystallization of the sample then occurs using the unmelted crystalline substrate as a seed.

Several different methods of examination have been used to show that for pulsed laser annealing melting actually occurs (Ref. 11,12,13,25, and 26). One method called time-resolved reflectivity (Ref. 11) has utilized the fact that the reflectivity of Si and GaAs increases when they are in a liquid state. Using a HeNe probe laser it was shown that an increase in the amount of the reflected HeNe beam did occur during the annealing laser pulse. The increase in reflectivity during the laser annealing for Si and GaAs was found to be comparable with the reported reflectivity values for crystalline and liquid Si and GaAs.

The solid-phase epitaxial regrowth differs from the liquid-phase in that the implanted layer does not melt. Work in the area of solid-phase epitaxial regrowth is being done at both Bell and Stanford Laboratories with a scanning cw laser beam (Ref. 2 and 13). Results obtained by Bell Laboratories found that cw laser annealing gives similar results as thermal annealing (Ref. 13). Bell Laboratories also performed experiments to verify that the regrowth procedure was solid-phase epitaxial regrowth and not liquid-phase. This experiment was done using a HeNe laser probe as in the time-resolved reflectivity measurements. These results can be seen in Figure 1 where the reflectivity measured below 6 W is that from an amorphous layer. At about 6.5 W the reflectivity drops to that of crystalline Si. As the power is increased,

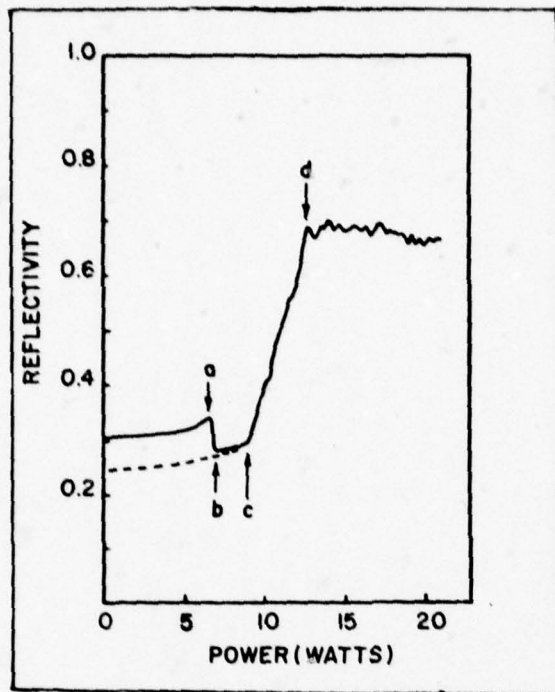


Figure 1. Reflectivity vs. Argon-Laser Power for Si:As 50 keV @ 10^{14} ions/cm² (Ref. 13:14).

a large change in reflectivity corresponding to Si melting is observed. The dashed line was recorded from a sample which was previously annealed. Comparison of the dashed line and the solid line supports the theory that the sample was annealed at power levels lower than that required to melt the sample; therefore, liquid-phase epitaxy was not the annealing mechanism. The work at Stanford (Ref. 27) also shows results of laser annealed samples to be similar to those of thermally annealed as seen in Figure 2. It can be seen in Figure 2 that the laser-annealed impurity distribution is almost identical to the distribution predicted by LSS range statistics. However, the thermal-annealed impurity distribution due to a heating time much longer than that of laser annealing is seen to have

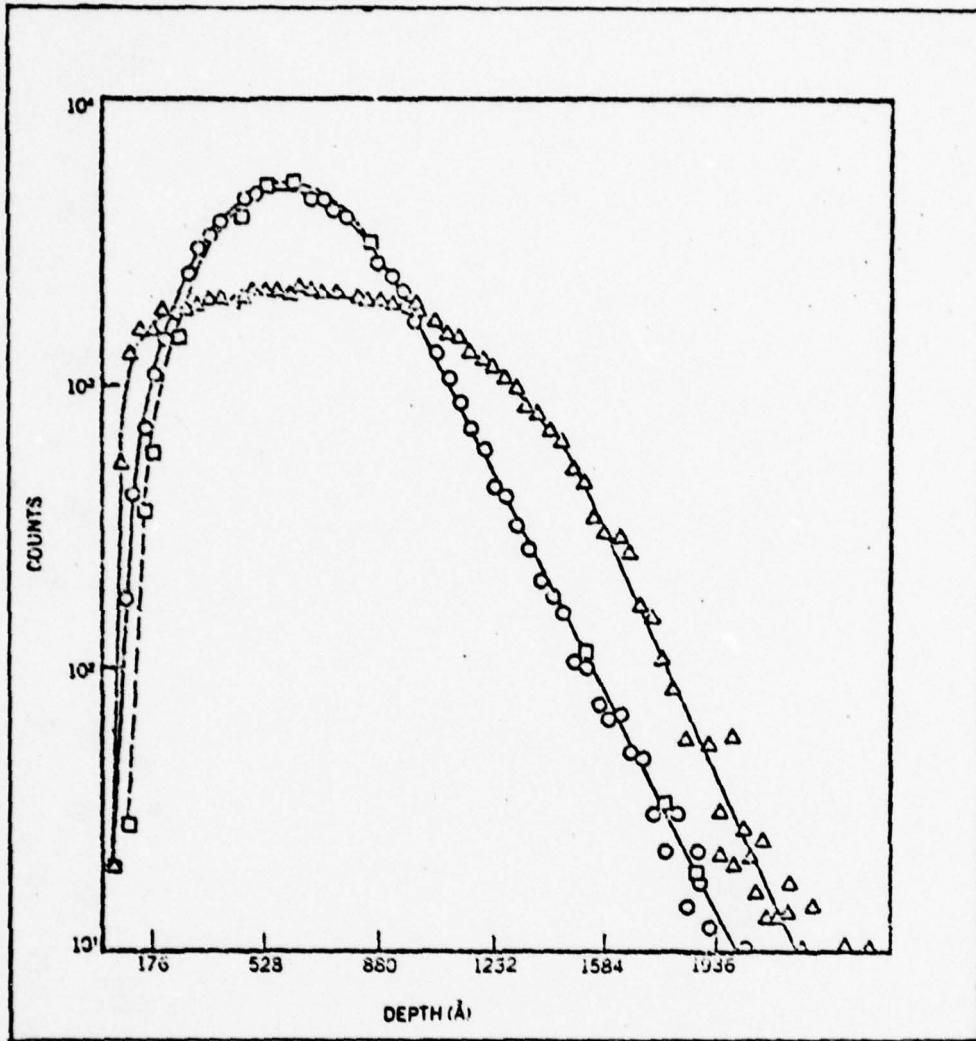


Figure 2. Concentration profiles of As in Si after laser annealing. Δ indicates the thermally annealed profile, \circ the laser annealed profile, and \square the calculated profile. (Ref. 27:276).

a broader distribution.

The majority of the laser annealing work has used nanosecond laser pulses. Because the process is so fast, many useful and interesting effects take place. Khaibullin, et.al. (Ref. 9:233) have stated that for the nanosecond regime the mechanism of laser annealing involves more than just ordinary thermal effects. They have also determined that for a high concentration of impurities the limit of solubility of the impurities in silicon can be exceeded. Another interesting result that has been suggested is that damage may result from a plasma breakdown in the vapors of the material. This suggestion is based on calculations showing that the pressure of the vapor for both Si and Ge at the energy density where damage is observed to occur is at about 10 atm (Ref. 16:637).

A problem with annealing GaAs has been that exposure to heat has resulted in a Ga-rich surface (Ref. 18 and 28). One method used to control the loss of As has been to cap the sample before annealing. It has been shown for uncapped GaAs that the concentration of the Ga at the surface is less when a nanosecond pulse is used than when a millisecond pulse is used (Ref. 28:3402). Bell Laboratories has also shown that by using time-resolved reflectivity and Rutherford Backscattering (RBS) that good crystallinity and minimal loss of As for the nanosecond pulse regime could be obtained. They also determined that the optimum for the melt time was dependent upon the concentration of implanted impurities (Ref. 18).

It has been determined that parameters such as the concentration of implanted impurities (Ref. 9 and 20), the

wavelength of the annealing laser (Ref. 9 and 13), and the substrate material (Ref. 13 and 16) affect the laser annealing process. Probably the most important parameter to be reported for a particular wavelength is the energy or power density used to anneal the sample. Several papers on laser annealing have reported changes in the physical or electrical properties of the material as a function of the energy or power densities used in the annealing process (Ref. 9,12,13, and 21). These papers have reported that at low energy densities no change occurred but at high energy densities visual damage such as craters, microcracks, and cavities in the surface began to appear. A problem with the reported information is that the values given for a particular change are not always consistent from paper to paper.

One reason for the differences in the reported information is the differences in the calibration of energy density used to anneal the samples. Another reason is that different groups have used different methods to examine changes in the physical or electrical properties. Although these different methods of examination are valid, there can be differences in what information can be obtained. For example, microscopy which can detect physical damage in the surface and optical reflectivity techniques which examine the crystallinity of the surface can give different ideas on what has happened to the surface of the sample. The optical reflectivity might reveal that the implanted layer is crystalline but the microscope might reveal that damage to the surface has also taken place. Also differences in the resolution of one microscope over another would lead to

differences in the energy density threshold at which surface damage would be detected.

In one of the papers, visual damage in implanted Si is reported to appear at about 35 MW/cm^2 for $\lambda = .69 \text{ }\mu\text{m}$ and 60 MW/cm^2 for $1.06 \text{ }\mu\text{m}$ (Ref. 9:226). However, in a paper from Bell Laboratories damage in implanted Si was at about 9.2 J/cm^2 or 306 MW/cm^2 for $\lambda = 1.06 \text{ }\mu\text{m}$ (Ref. 13). The reason for the difference between these two reported values for damage could be in the way damage was defined. The value reported by Khaibullin, et.al. (Ref. 9:226) for damage was determined by examination with an electron microscope. Bell Laboratories; however, used the value of the energy density at which there was a loss of the time-resolved reflectivity signal. The spot size of the HeNe probe beam on the sample was $.3\text{mm}$ (Ref. 11:438); therefore, the amount of surface damage required to lose the reflectivity signal would be much larger than that required to form small craters in the surface of the sample. Much of the discrepancy in the energy density needed to produce damage in the sample could be due to the method used to detect the damage and in the definition of damage.

Time-Resolved Reflectivity

Time-resolved reflectivity is a method used to examine the melting that takes place in the surface of a sample as it is being annealed. To accomplish this examination, a cw laser, usually HeNe, is reflected from the surface of the sample that is being annealed. As the sample melts its reflectivity increases. The change in reflectivity as detected by a fast

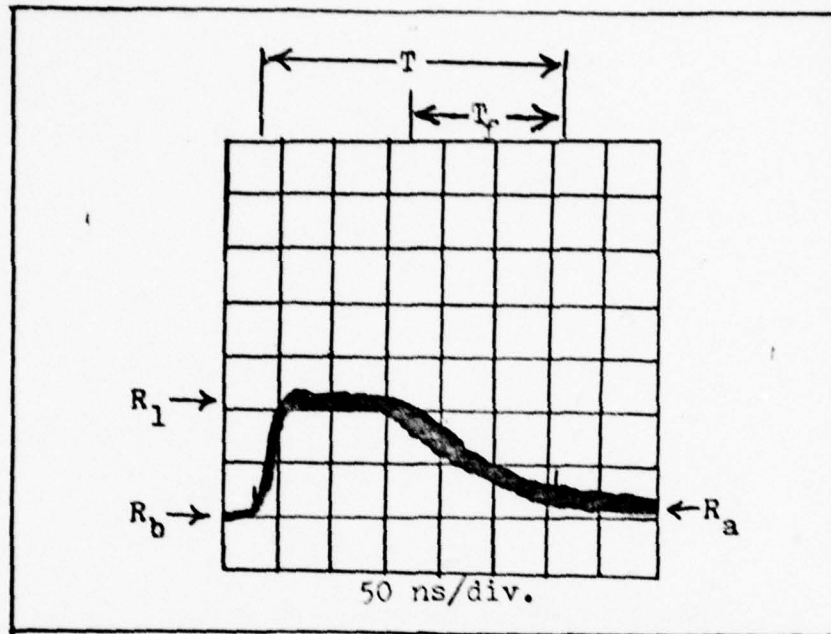


Figure 3. Time Resolved Reflectivity Trace for virgin GaAs.

photodiode can be seen in Figure 3.

The quantity R_b in Figure 3 corresponds to the reflectivity of the solid surface before annealing. The value of R_b at $\lambda = .63 \mu\text{m}$ is 35% and 33% at room temperature for virgin Si and GaAs respectively (Ref. 29:523). Amorphous Si has a reflectivity of 45% (Ref. 30:648), and GaAs implanted at 10^{14} ions/cm² has a reflectivity of 37% (Ref. 21:578). As the sample heats, the reflectivity will increase until it reaches a value R_1 which corresponds to the reflectivity of a liquid melt at least one optical depth thick. The value of R_1 at $\lambda = .63 \mu\text{m}$ is 74% for liquid Si at 1600⁰ C and the optical depth given by the reciprocal of the absorption coefficient (α^{-1}) is 112 Å (Ref. 31:2111). The reflectivity will remain at the value R_1 until the melt depth due to recrystallization

becomes less than one optical depth. As recrystallization continues and the surface temperature decreases, the reflectivity will drop to R_a which is the reflectivity of the solid after annealing.

Little information was found on the reflectivity of Si or GaAs as a function of temperature from 300° K to the melting point. References to information on the reflectivity for Si and GaAs for different wavelengths and temperatures can be found in Appendix A. In one paper the reflectivity of Si was reported to increase to 60% just below the melting point (Ref. 32:138); however, another paper stated that the reflectivity was only 37.5% at the melting point (Ref. 33:319). Due to the lack of information of the reflectivity as a function of temperature, an exact interpretation of Figure 3 is not possible. Bell Laboratories in one paper interpreted the time that the material was in a melted or liquid state (T) to be just the flat portion of the signal shown in Figure 3 (Ref. 11:439). In a more recent article they have interpreted T to be the time from R_b to R_a (Ref. 13:16). In this last article, Bell Laboratories has also interpreted the fall time (T_f) in Figure 3 to be the length of time required for one optical depth to recrystallize. The value of T_f can then be related to the velocity that the melt-solid interface moves toward the surface of the sample. Bell Laboratories also found T_f to be dependent upon minute dust particles and other surface irregularities (Ref. 13:22).

In Figures 4-9 the time-resolved reflectivity signal from virgin GaAs at different energy densities is shown. Figure 4

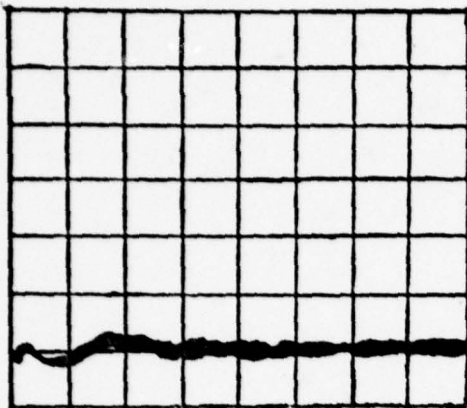


Figure 4.

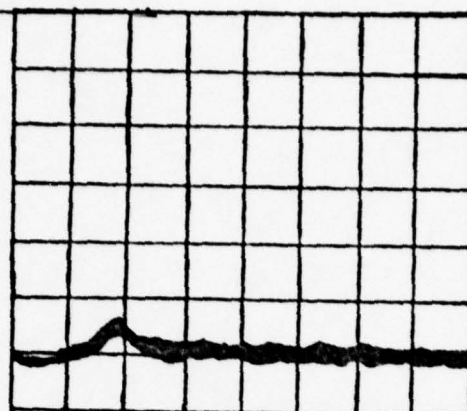


Figure 5.



Figure 6.

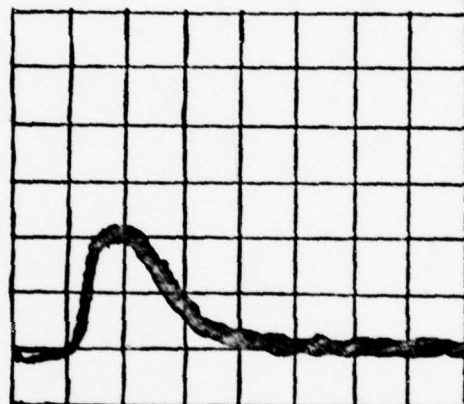


Figure 7.

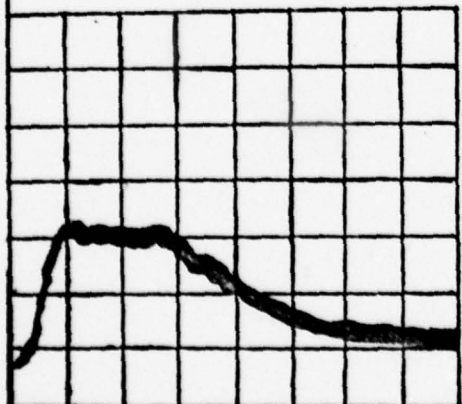


Figure 8.

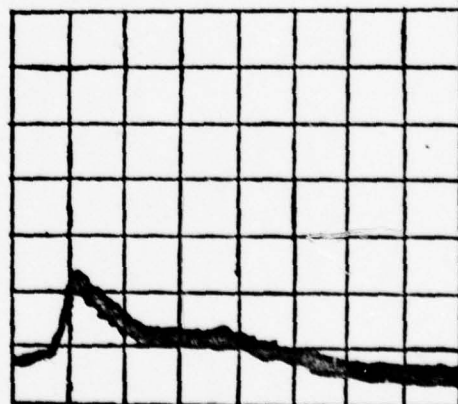


Figure 9.

Figures 4-9. The HeNe reflected signal from virgin GaAs at energy densities of .2, .24, .36, .5, .75, and .95 J/cm², and melt times of 0, 47, 77, 127, 250, and 280 (?) nsec respectively.

shows that at $.2 \text{ J/cm}^2$ no melting of the surface occurred. As the energy density was increased the reflected signal became larger until, as shown in Figures 4 and 5, the height of the reflectivity signal reached a maximum corresponding to R_1 in Figure 3. As the energy density was increased from Figure 4 to Figure 5, the flat portion of the signal becomes longer. Finally, the energy density will become so large that the surface of the sample will be destroyed, and a signal like Figure 6 will be obtained.

By plotting T versus energy density, characteristics such as the difference in the energy density required to start melting in implanted and virgin samples can be obtained. T has been compared to observed changes in samples by RBS to determine the optimum conditions for annealing GaAs (Ref.18). Therefore, T can be related to the physical or electrical changes in the material as a result of the annealing process in the same way that the energy density has been used (Ref. 9,19, and 21).

Laser Absorption During Annealing

Due to the absorption of the laser energy, the temperature of the sample will increase during the annealing process. As the temperature increases the atomic mobility of the atoms in the semiconductor will increase allowing the impurity atoms to move into substitutional lattice sites.

Most of the theoretical examination of the absorption of the laser radiation has dealt with crystalline semiconductors. One of the most important parameters that must be considered when examining the absorption in crystalline semiconductors is

the photon energy ($h\nu$). For an $h\nu > E_g$, the laser energy will be strongly absorbed as in metals. However, if $h\nu < E_g$, the absorption will be governed by multiphoton absorption and by extrinsic material properties such as impurities, inclusions, and surface preparations (Ref. 4:1). The measured absorption coefficients (α) for slightly disordered and amorphous Si bear out this fact.

Khaibullin, et.al. (Ref. 9:227) report that for $h\nu > E_g$ ($\lambda = .69 \mu\text{m}$) slightly disordered Si $\alpha_{.69 \mu\text{m}} = 4 \times 10^3 \text{ cm}^{-1}$, and for amorphous Si $\alpha_{.69 \mu\text{m}} = 4 \times 10^4 \text{ cm}^{-1}$ or an increase of an order of magnitude. For $h\nu \approx E_g$ ($\lambda = 1.06 \mu\text{m}$) slightly disordered Si $\alpha_{1.06 \mu\text{m}} = 20 \text{ cm}^{-1}$, and for amorphous Si $\alpha_{1.06 \mu\text{m}} = 4 \times 10^4 \text{ cm}^{-1}$ or an increase in α of three orders of magnitude. Therefore, it can be seen that the effect of the extrinsic material properties on α is much larger for $h\nu \approx E_g$ than when $h\nu > E_g$. The importance of the extrinsic properties of the material when $h\nu \approx E_g$ is also seen from reported information that it is difficult to obtain uniform annealing in Si when $1.06 \mu\text{m}$ irradiation is used (Ref. 17:558).

Khaibullin, et.al. (Ref. 9:231) state that if the wavelength of the laser used for annealing is in the fundamental absorption band then two mechanisms for absorption dominate: (1) a semiconductor mechanism and (2) an induced metallic mechanism. The semiconductor mechanism is a band-to-band absorption, and results whenever photons having energy $h\nu > E_g$ are absorbed and generate electron-hole pairs. When these electron-hole pairs recombine in a nonradiative process, the absorbed energy is transferred to the lattice causing it to

heat. The metallic mechanism takes place whenever the energy is absorbed by free electrons. The photon energy absorbed by the electrons goes into kinetic energy and is transferred from the electrons to the lattice by collisions which results in the heating of the lattice. According to Kruer, et.al. (Ref. 4:2), the band-to-band generation is usually the dominant mechanism whenever $h\nu > E_g$. However, for nanosecond pulses the metallic mechanism can be very important since the material melts. Once the material melts, $h\nu$ does not need to be greater than the energy gap of the sample to be effectively absorbed. Bell Laboratories have shown that the optical properties of the melted material are metallic since both infrared and visible laser irradiation are absorbed with about the same efficiency (Ref. 17:558).

One of the problems with the published theoretical work is that crystalline samples are considered. At energy densities below that required to achieve melting, factors such as the reflectivity and the absorption coefficient of implanted and crystalline samples are usually different. Using time-resolved reflectivity techniques, the energy density required to start melting (melting threshold) in Si implanted with 30 keV As at 10^{15} ions/cm² with $\lambda = .53 \mu\text{m}$ was determined to be about 2/3 that required to produce melting in unimplanted Si (Ref. 13:20). The reason for the difference in melting threshold is not known but lower melting temperatures or thermal conductivity, or both have been suggested (Ref. 13:20). Other factors that might also produce the lower melting threshold are the difference in reflectivity and absorption coefficient of the

implanted and unimplanted Si.

Although a difference exists in the threshold for melting between implanted and unimplanted Si, the difference in the melt time (T) rapidly disappears as the energy density is increased (Ref. 13:17). Since the sample is in a melted state, the dominant absorption mechanism is no longer a band-to-band absorption but a metallic absorption. Therefore, the reason T becomes the same for both implanted and unimplanted Si is that the mechanism for absorption and the reflectivity will be the same. As the energy density is increased above the melting threshold, the percentage of energy absorbed prior to melting will decrease making the difference in T between the implanted and unimplanted samples decrease.

Plasma Surface Damage

One possible cause of damage such as craters in the surface of a laser annealed sample that has been suggested is that the damage might be due to a plasma formed at the air-sample interface (Ref. 16:637). The formation of a plasma can result in an enhanced coupling of the laser energy to the surface of the sample (Ref. 35:70). Although the mechanisms for the igniting of a plasma are not well understood, possible causes are thermionic emission and vaporization of surface particles (Ref. 35:69). The reason for the suggestion that damage was due to a plasma is that the vapor pressure of the vaporized surface particles in Ge and Si, where damage was observed to occur, was calculated to be 10 Atm (Ref. 16:637). Comparison between reported information is needed to determine whether or

not a plasma will be formed.

The energy or power density required to produce a plasma in air (air breakdown) depends upon the ambient gas, the pressure, the laser wavelength, the focal spot size, and partly on the pulse length and distribution of the intensity across the laser beam (Ref. 34:65). An example of how pressure, ambient gas, and wavelength affect the breakdown threshold can be seen in Figure 10. This work was done using the first and second harmonics of ruby and neodymium lasers. The pulse length for $\lambda = 1.06 \mu\text{m}$ and $.69 \mu\text{m}$ was 40 nsec, while $\lambda = .53 \mu\text{m}$ and $.374 \mu\text{m}$ had pulse lengths of 28 and 20 nsec respectively.

Buscher, Tomlinson, and Damon (Ref. 34:66) have also measured the breakdown threshold for several molecular and inert gases using 40 nsec pulsed ruby and neodymium lasers. From these results seen in Figure 11, the breakdown threshold in air at 760 torr (1 atm) is about $2 \times 10^{11} \text{ W/cm}^2$ and $6.5 \times 10^{10} \text{ W/cm}^2$ for $\lambda = .69 \mu\text{m}$ and $1.06 \mu\text{m}$ respectively.

Khaibullin, et.al. (Ref. 9:226) reported observing damage in Si at $3.5 \times 10^7 \text{ W/cm}^2$ for $\lambda = .69 \mu\text{m}$ and $5.8 \times 10^7 \text{ W/cm}^2$ for $\lambda = 1.06 \mu\text{m}$. Therefore, from Figure 11 air-breakdown occurs at about three orders of magnitude more than the damage threshold reported by Khaibullin, et.al., and at about two orders of magnitude more than Bell Laboratories reported damage threshold value.

For laser beams striking a solid surface, plasmas have been observed to occur at more than two orders of magnitude below that required for air-breakdown (Ref. 30:6,7). A factor of two orders of magnitude lower would place plasma formation

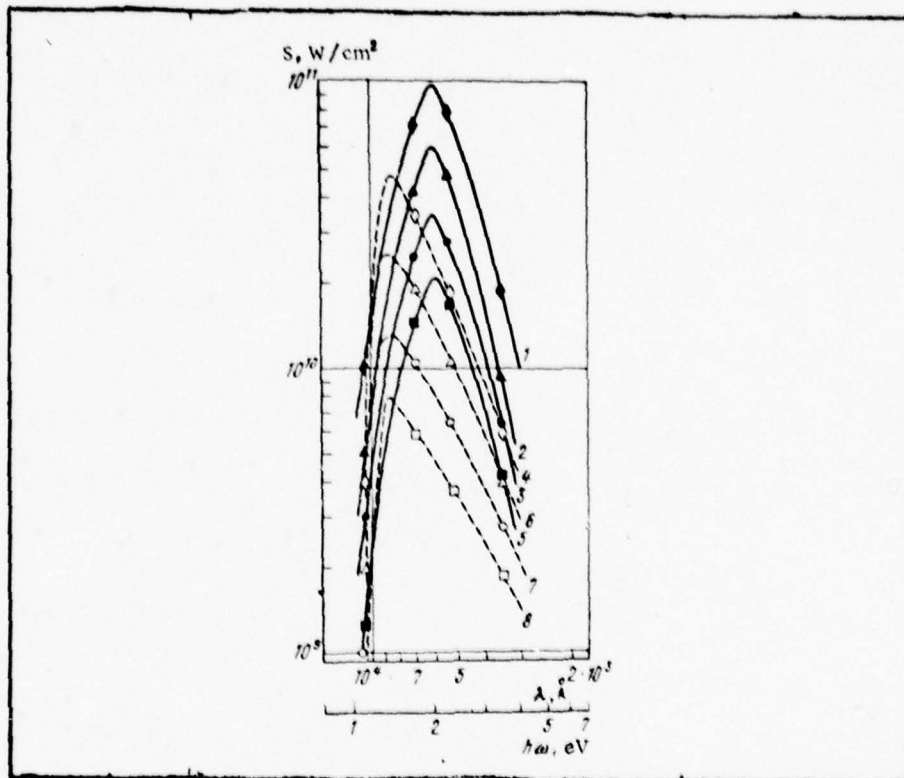


Figure 10. Frequency dependences of the breakdown thresholds of inert gases (Ref. 34:74): 1-3, 5) argon; 4, 6-8) xenon; 1, 4) $p=1000$ torr; 2, 6) 2000 torr; 3, 7) 4000 torr; 5, 8) 8000 torr.

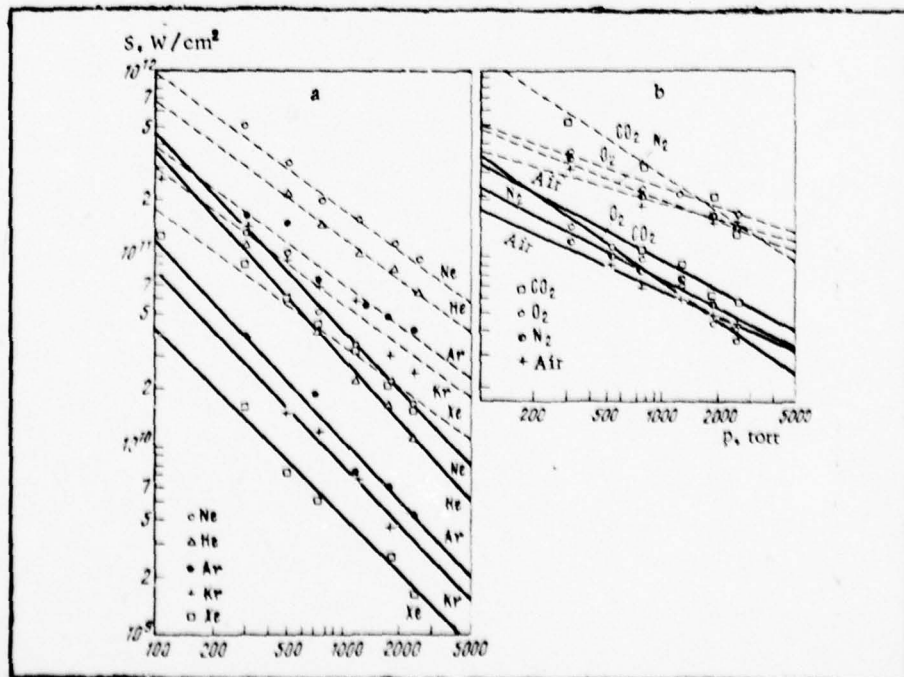


Figure 11. Threshold power densities in the breakdown of molecular (a) and inert (b) gases (Ref. 34: 66). The dashed lines represent the effects of a ruby laser, and the continuous lines the effects of a neodymium laser.

for $\lambda = 1.06 \mu\text{m}$ at about $6.5 \times 10^8 \text{ W/cm}^2$ which is close to the damage threshold reported by Bell Laboratories. Therefore, the suggestion that damage is due to a plasma formed at the air-sample interface is valid and should be investigated. Methods that have been used to verify that a plasma has been formed in air or on metal targets such as Aluminum (Al) are a visible flash, a decrease in laser energy transmitted through the focal volume, or an increase in reflection of the laser radiation (Ref. 34:64,72).

Theoretical Work on Laser Annealing

The purpose of a theoretical treatment of laser annealing is that it can be used to obtain a better understanding of the heating and melting effects that take place. To obtain a detailed analysis of the effects of heating, the heat flow equation must be solved for the case where the heat capacity (C_p), the mass density (ρ), and the thermal conductivity (K) are temperature dependent. The heat flow equation

$$\nabla^2 T - (1/D)\partial T/\partial t = -A(x,y,z,t)/K$$

where the thermal diffusivity (D) = $K/C_p \rho$ and $A(x,y,z,t)$ is the heat generation rate, becomes nonlinear when C_p , ρ , and K are temperature dependent and most of the time must be solved numerically (Ref. 36:10).

Several numerical solutions of the heat flow equation have been performed for laser annealing of semiconducting material with nanosecond pulses (Ref. 32,32,37, and 38). To simplify the calculations, the heat flow equation can be reduced to one dimensional by assuming that the radius of the laser beam

is much larger than the thermal diffusion length $(2Dt_p)^{\frac{1}{2}}$, where t_p is the pulse length of the laser. Using the one dimensional heat flow equation, the numerical solutions were performed by dividing the sample into slices Δz thick and the time into a number of small time intervals Δt long. The solutions were then obtained by using an iterative process for each cell and time Δt . The latent heat of fusion at the melt-solid interface and estimates of how K , C_p , ρ , α , and the reflectivity (R) changed with changing temperature were also included. However, estimates of how R and α changed differed from paper to paper.

One of the purposes of the numerical work was to determine whether liquid or solid-phase epitaxy was the regrowth mechanism. Since the diffusion coefficient for solid Si is about 10^{-12} to 10^{-14} cm^2/sec , solid-phase epitaxy can not explain the regrowth that has been observed (Ref. 32:137). However, liquid Si has a diffusion coefficient of about 10^{-4} cm^2/sec and so the growth rate could be as high as 10^{10} $\text{\AA}/\text{sec}$ which could explain the regrowth observed (Ref. 38).

The result of numerical solutions have shown that for nanosecond pulses the material does melt and that the depth of melt is dependent on the energy density (Ref. 32,33,37,and 38). These results agree with experimental work that has shown that the material melts (Ref. 12 and 13) and that the regrowth mechanism is a liquid-phase epitaxy for laser annealing with nanosecond pulses.

Baeri, et.al. (Ref. 38) have performed numerical calculations for the temperature of the surface layer of an amorphous Si versus time for a flat and gaussian laser pulse. They have

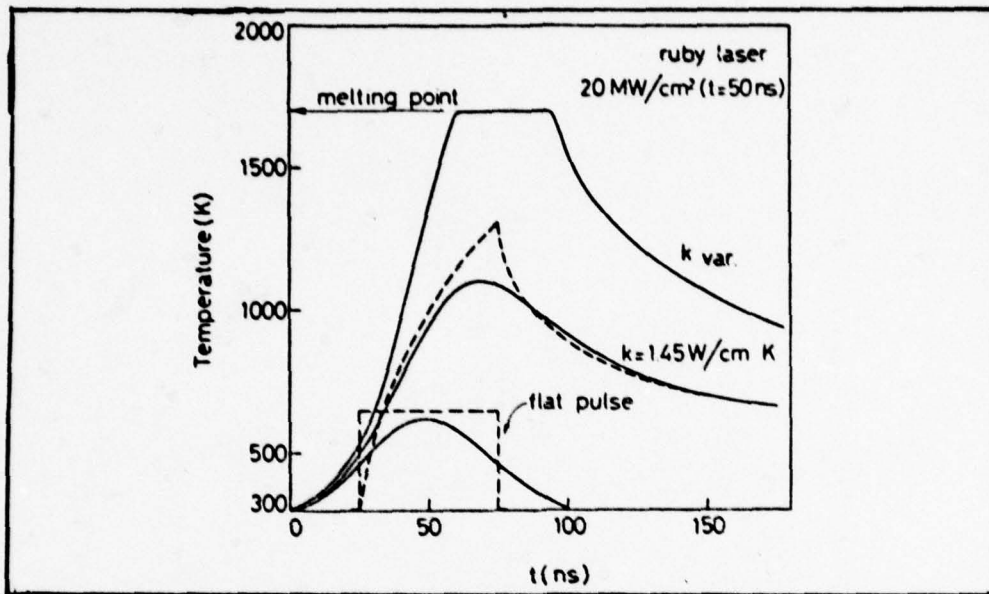


Figure 12. Calculated surface layer temperature of amorphous Si vs. time for a flat and a Gaussian laser pulse shape. Lower curves for room temperature thermal conductivity (K) and upper curve for a variable K. (Ref. 38)

also shown in Figure 12 that for a variable K the surface of the material will melt but for K at room temperature the material will not melt.

Some of the results of Bell, et.al. (Ref. 33) can be seen in Figures 13 and 14. In Figure 13 the temperature versus depth in the sample is plotted for different times during the laser pulse. At the melting temperature (T_m) the temperature rise is interrupted until the latent heat of fusion can be added to cause the phase change from solid to liquid. It can also be seen that the material is still in a liquid phase when the pulse is finished.

In Figure 14, the depth of melt versus incident energy density is plotted for several different materials. From Figure 14, it can be seen that amorphous Si melts at a lower energy density than that of virgin Si. The difference

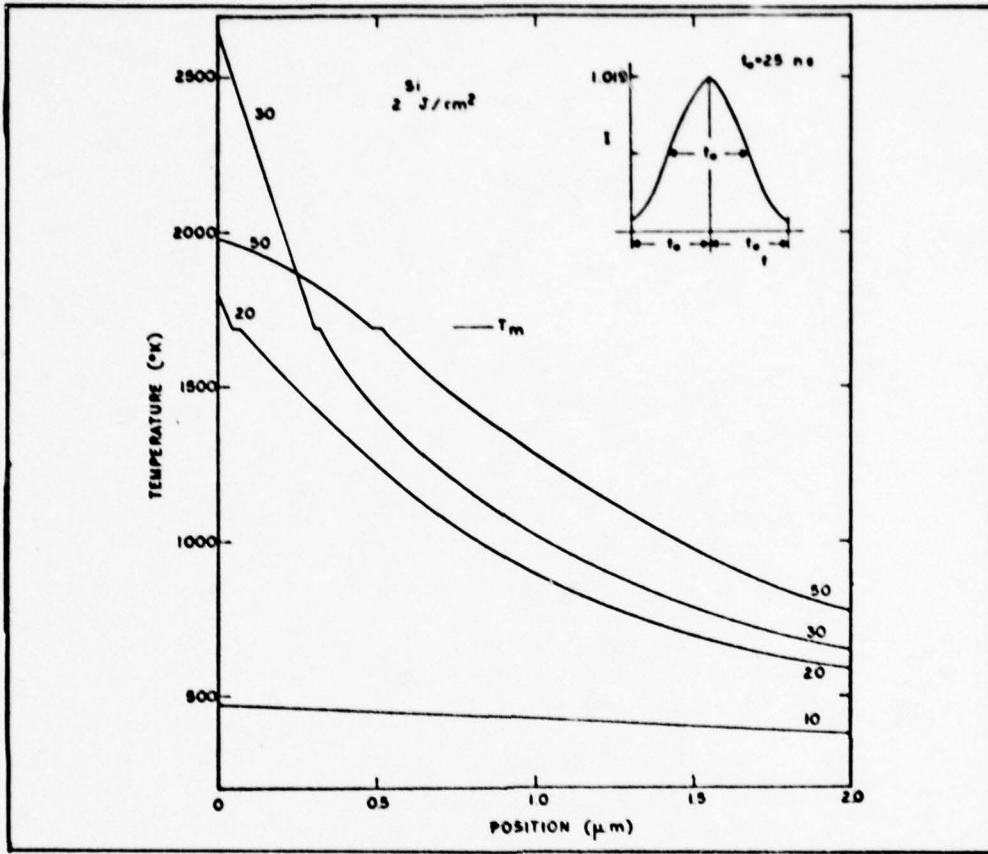


Figure 13. The predicted position dependence of temperature at different times during the laser pulse (ns) for virgin Si. (Ref. 33:316)

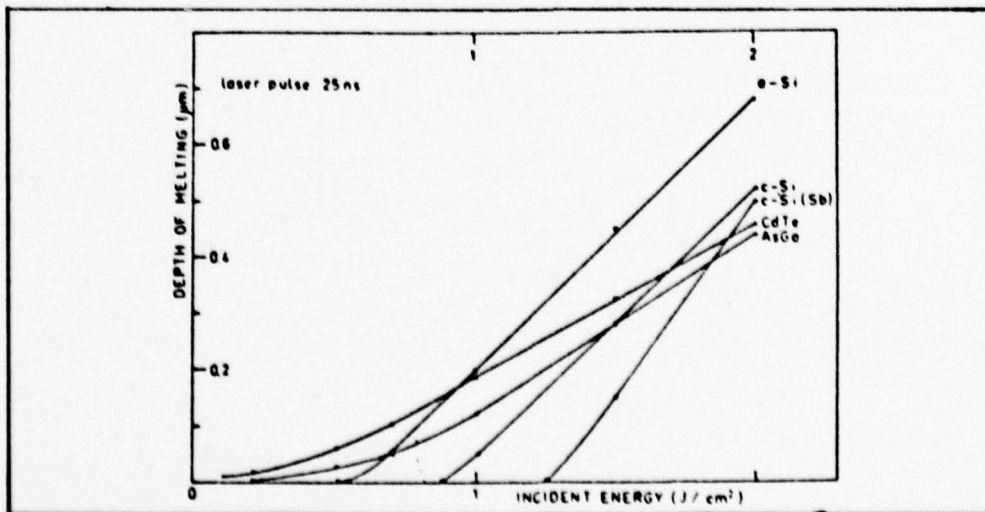


Figure 14. Depth of melting as a function of incident energy from a ruby laser having a pulse width of 25nsec. (Ref. 33:319)

observed for the amorphous and virgin Si is due to a difference in the absorption coefficient (α). From Figure 14 it can also be seen that GaAs melted sooner than Si and the slope of the melt depth versus energy density is smaller than Si. The differences between Si and GaAs are caused by the differences in C_p , ρ , K , R , and α for the two materials. The values that were used for GaAs are not ; therefore, the quantities that contributed the most to the difference can not be determined.

III. EXPERIMENT

Equipment and Experimental Arrangement

The laser used for this experiment was a Holobeam series 300 ruby laser equipped with a 3/8 in. by 3 in. long ruby rod, and pumped with a Xenon-filled arc discharge lamp. The laser was operated in the Q-switch mode with an output that can exceed 100 MW. A 60 cm long cavity was used for all experimental work, and the measured pulse width at half maximum (FWHM) was 27 to 30 nsec. The output of this ruby laser is multimode and horizontally polarized.

Two HeNe lasers were used in the experimental set up which can be seen in Figure 15. One HeNe laser was used for alignment purposes, while the other was used for the time-resolved reflectivity measurements (Ref. 10, 11, and 18).

The HeNe laser used for the time-resolved reflectivity measurements was not polarized, and had an output of 2 mW in the TEM₀₀ mode. The diameter of the HeNe beam on the sample was .72 mm, and the angle of incidence of the laser beam on the sample was 36°. The beam reflected from the sample was monitored by a MRD-500 photodiode made by Motorola Semiconductor Products, Inc. The photodiode was placed behind a .63 μm transmission filter and a pinhole so that the ruby laser pulse would not affect the signal detected by the photodiode. The photodiode has a rise time of about 2 nsec. The voltage across this resistor was monitored with an oscilloscope whose rise time was 3.5 nsec.

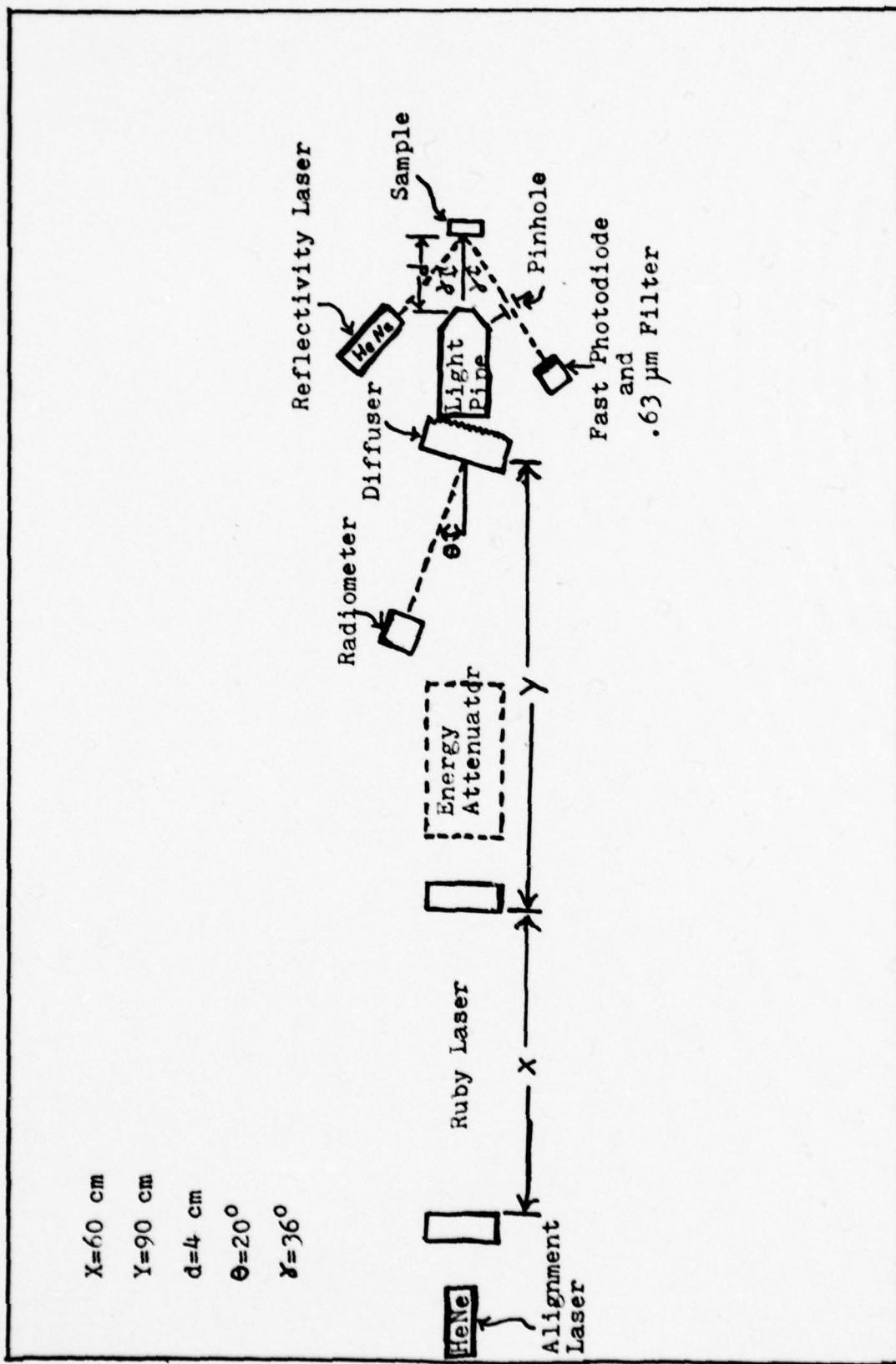


Figure 15. Experimental Setup

For laser annealing, the spatial homogeneity of the laser beam is important (Ref. 24). Since the ruby laser operation is multimode, the spatial homogeneity is not uniform. To improve the homogeneity, a piece of glass which was frosted on one side was used as a diffuser. Two different diffusers, a lightly frosted diffuser for annealing Si and a heavily frosted diffuser for GaAs, were made for this process. Both were frosted with Buehel Aluminium Oxide 600 grit powder placed on a piece of 600 grit paper. The lightly frosted diffuser was made by mixing the 600 grit powder with enough water to make a liquid suspension, while the heavily frosted diffuser was made by mixing only enough water to make the powder into a paste. Light sensitive paper was used to examine the spatial characteristics of the ruby laser beam transmitted through the diffuser. The burn patterns on this paper showed the spatial homogeneity from the heavily frosted diffuser to be more uniform; however, the energy density transmitted was about 50% less than the lightly frosted diffuser. The diffuser was mounted at an angle of 10° from the ruby beam with the frosted side closest to the sample. The unfrosted surface was facing away from the sample, and could be used as a reflector so that the energy density used to anneal the samples could be monitored.

The monitoring of the energy density was done with a radiometer. The reading from the radiometer was a measurement of the amount of energy reflected from the front surface of the diffuser. This reading was then related to the energy density at the sample. The energy density was measured with an energy

receiver which was placed behind a 4 mm aperture. Pulses from the milli-joule range to 1000 joules can be detected by the energy receiver which senses a rise in temperature of the receiving unit and compares it with the ambient temperature. The accuracy of the energy measurements is $\pm 3\%$. The energy receiver is also equipped with a Hewlett Packard 4220 fast photodiode (rise time of approximately 2 nsec) for measuring the pulse width of the laser.

To examine the effects of laser annealing, it is necessary to be able to change the energy density. This could be accomplished by changing the Xenon pump voltage; however, this also changes the laser pulse width. To make it possible to change only the energy density, the Xenon pump voltage was kept constant and part of the laser beam was attenuated. Attenuation was accomplished by using pieces of glass to reflect part of the laser energy into an energy dump.

To protect the ruby laser, the total energy output was kept below 1.5 J. Due to the energy loss caused by the diffuser and non-homogeneity of the laser beam, an aluminum light pipe was used. The interior of the pipe was polished with a cotton swab and the same 600 grit powder used to frost the glass diffusers. The light pipe was mounted directly behind the glass diffuser, and it was found that by using the light pipe it was possible to get the energy density greater than one joule per square centimeter. However, due to spectral reflections, the annealing beam profile or the energy density as a function of distance from the center of the beam changed depending upon the distance from the end of the light pipe. From burn patterns

and from measuring the energy density across the annealing beam, it was found that 4 cm behind the pipe gave the most uniform beam profile. Examples of this can be seen in Appendix B. This position was then chosen as the place for the sample to be annealed.

Experimental Procedures

The first thing that was done was to align the ruby laser with an autocollimator. Sometimes the alignment of the cavity would change and the cavity would be realigned. The need for realigning the cavity was determined by observing a drop in energy or an increase in pulse width as detected by the radiometer.

After the ruby laser cavity was aligned, light sensitive paper was used to make a burn pattern of the output of the ruby laser. The burn pattern was then used to position the HeNe alignment laser so that it was traveling the same path as the ruby laser beam. The alignment laser was then used to align the diffuser, the sample, the radiometer, and the time-resolved reflectivity laser.

The alignment of the items above was relatively stable and did not need to be changed from pulse to pulse. However, when the energy density was changed by using the energy attenuator, these items needed to be realigned. The reason this realignment was necessary was because of the displacement in the ruby laser beam caused by the tilted pieces of glass used in the attenuator.

Each time the light pipe was realigned, a burn pattern on light sensitive paper placed 10 cm from the end of the pipe was

taken. This burn pattern was used to determine whether or not the light pipe was properly aligned. If it was properly aligned, the burn pattern would appear as a dark ring with a dark burn spot in the center. If the light pipe was not properly aligned, the burn spot would not be in the center of the ring.

After the system was aligned, the 4 mm aperture and the energy receiver were used to measure the energy density. The aperture was positioned in the center of the ruby laser beam, 4 cm behind the end of the light pipe. The energy receiver was positioned directly behind the aperture. Four to six laser pulses were then measured with the radiometer and the energy receiver, and an average ratio of these two readings was calculated. The ratio was compared with the calibrated results to see if any change in the ratio had occurred. During the time of the experimental work, no change in the ratio occurred.

Calibration and Reproducibility

To be able to examine the results and make comparisons with reported work, an accurate measure of the energy density and the laser pulse width used to anneal each sample was needed.

The pump voltage on the Xenon-filled arc lamp was kept constant during the experiments, and only a small fluctuation in the laser pulse width was observed. The average pulse width of the ruby laser was measured to be 28 nsec (FWHM).

In order to avoid calibrating the attenuator and because of variations in the output of the ruby laser, it was necessary to measure the energy density for each laser pulse. The radiometer was used for this purpose. The radiometer measured the

amount of energy reflected by the front surface of the diffuser; therefore, a calibrated ratio of the energy density 4 cm behind the light pipe divided by the energy measured with the radiometer was needed to convert the energy measured by the radiometer to energy density on the sample. To measure the energy density 4 cm behind the end of the light pipe, a 4 mm aperture with the energy receiver was used. The energy detected by the energy receiver was then multiplied by the area of the aperture to get the energy density.

An assumption used in making this calculation was that the energy density across this 4 mm aperture was approximately constant. From burn patterns and measurements of the beam profile found in Appendix B, it can be seen that this assumption is valid. Using the information obtained from the beam profile measurement, the energy density changes less than 10% over the 4 mm area. The beam profile measurement was done with a 1.4 mm aperture, and is just an approximation.

Assuming that the energy density measured with the 4 mm aperture is a good approximation, the ratio of energy density at the sample divided by the reflected energy can be obtained. This ratio was determined to be $.173 \pm .001 \times 10^{10}$ (J/cm²-coulomb) when the lightly frosted diffuser was used. When the heavily frosted diffuser was used the ratio was $.0870 \pm .0002 \times 10^{10}$ (J/cm²-coulomb). However, differences of up to 8% from these average values were measured. The major reasons for this 8% difference in the measurements were misalignment of the light pipe and inaccurate energy density measurements resulting from the energy receiver not being allowed to thermalize properly.

To minimize the effects of this inaccuracy, the first laser pulse was not used to get the average, and at least five minutes were allowed for the energy receiver to thermalize between each laser pulse.

The energy receiver was calibrated with a TRG 108 thermopile. From that calibration the energy measured by the energy receiver was only 80% of that measured with the thermopile. The accuracy of the thermopile is not known.

Each time a sample was annealed the energy density and a picture of the time-resolved reflectivity signal were recorded. From this picture the melt time (T) of the sample could be established. In determining T a criteria of full width at 90% of the maximum height was used. Accuracy of T was ± 7 nsec due to errors in the measurements.

Samples

The samples that were used for the experiment were virgin GaAs compensated with chromium (Cr), virgin Si, GaAs implanted with 120 keV tellurium (Te) and argon (Ar) at 10^{14} ions/cm², and indium (In) at 10^{15} ions/cm². The implanted samples were cleaned with dehydrated alcohol and blown dry while the virgin Si samples were cleaned in hydro-fluoric (HF) acid and then washed in dehydrated alcohol and blown dry. The method used to clean the virgin GaAs was to wash the sample in hydrochloric acid and then water. The virgin GaAs samples were then etched for one minute in a solution of three parts H₂SO₄, one part H₂O₂, and one part H₂O at room temperature. The rate of this etching solution was 10 μ m/min. The samples were then cleaned

with dehydrated alcohol and blown dry.

The reason for using the HF acid on the virgin Si and the etching solution on the virgin GaAs was to remove any oxides that were on the surface of the samples. Efforts to remove the oxides from the implanted samples were not made because part of the implanted layer would have also been removed. The methods that were used to clean both the virgin and implanted Si and GaAs gave a clean surface which is needed for the annealing process.

Analysis of Annealing

Analysis of the annealing was done using time-resolved reflectivity measurements, and optical reflectivity. The time-resolved reflectivity measurements were used to determine how long the sample was in a melted state. These measurements were then compared with results obtained with the optical reflectivity techniques performed by Lt. Mullins. A detailed description of the optical reflectivity technique can be found in Reference 22.

Error Analysis

Error analysis is used to determine the accuracy of the experimental data. The analysis is separated into the errors in the measurement of the melt times (T) and the errors in the measurement of the energy density.

The measurements that were performed on T used the full width at 90% of the height of the signal from the fast photodiode. Since the value of T is related to the physical or electrical changes that occur in the material by other techniques,

only the errors in the difference of T from sample to sample are of interest. Therefore, if T is large compared to the rise time of the oscilloscope (3.5 nsec) and the rise time of the fast photodiode (2 nsec) only errors due to the measuring of the length of T will be considered. The error in the measurement of the length of T was determined to be ± 7 nsec.

Errors in the measurement of the energy density result from the beam profile, the accuracy of the energy receiver, and the ratio of the energy density incident upon the sample to that reflected into the radiometer. The beam profile was found to change about 10% over a 4mm area as shown in Appendix B. The accuracy of the energy receiver was given as 3% and the ratio of the energy density incident upon the sample to that reflected into the radiometer had a deviation of 1%. The error in the energy density measurements is then taken to be 13%. The accuracy of the measurements is not known since the energy receiver was not calibrated against a calibrated energy meter. Therefore, the error of 13% is just the possible error in the energy density measurement from one sample to the next.

IV. RESULTS AND DISCUSSION

Laser Annealing of GaAs

The GaAs samples were annealed with a ruby laser ($\lambda = .694 \mu\text{m}$) and pulse width of about 28 nsec (FWHM). The energy density used for annealing was varied from $.09 \text{ J/cm}^2$ (3.2 MW) to $.95 \text{ J/cm}^2$ (34 MW). Analysis of the effect that the energy density had on the samples was done with time-resolved reflectivity (Ref. 11 and 13), visual microscopy, and optical reflectivity techniques (Ref. 22).

Results from the time-resolved reflectivity measurements for implanted and virgin GaAs can be seen in Figure 16. Measurements obtained by Bell Laboratories (Ref. 13:17) using GaAs implanted with 50 keV Te at $10^{16} \text{ ions/cm}^2$ and annealed with $\lambda = .530 \mu\text{m}$ are also shown.

The interpretation of the melt time (T) in Figure 16 was found to affect the shape of the T versus energy density curve. Measuring T as the flat portion having a reflectivity R_1 in Figure 3 gave poor results. These results showed large changes in T for samples annealed at approximately the same energy density. These inconsistencies are similar to those that have been reported (Ref. 11:438). Measuring T as the length of time from R_b to R_a in Figure 3 was not always possible due to the electrical noise in the reflectivity signal. Measurements from R_b to R_a on the implanted samples gave a curve very close to that of Bell Laboratories in Figure 16. Accuracy of the measurements made from R_b to R_a of the implanted samples is questionable because of the noise problem. Due to problems

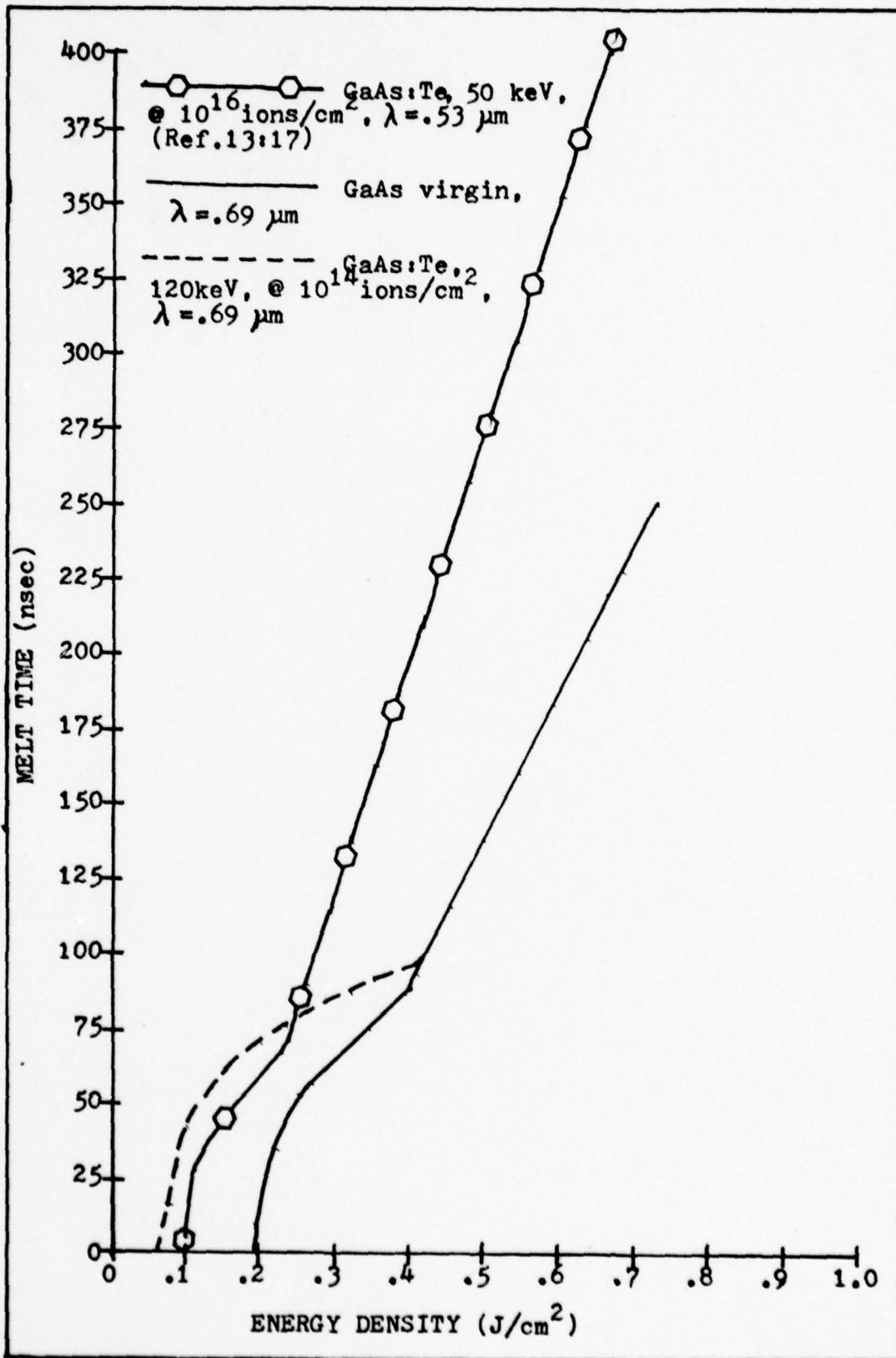


Figure 16. Melt Time of GaAs vs Energy Density

with the noise and the poor results obtained from measuring the flat portion of the reflectivity signal, the measurement of T used in Figure 16 was obtained by taking the full width at 10% of the height above R_b and R_a . Since information was not found on the reflectivity of semiconducting materials as a function of temperature, it was not possible to determine whether or not T actually represents the time that the material was melted.

To determine whether or not melting occurred, voltage measurements were taken for values of R_a and R_1 from the reflectivity signal. Using the change in voltage from R_a to R_1 and a value of 34% for R_b (Ref. 29:522), the value of R_1 was determined to be approximately 59%. The value of R_1 obtained from the voltage measurements is smaller than that measured for liquid Si by about 15% (Ref. 31:2111). However, the value of R_1 obtained is probably that of liquid GaAs, and the difference between R_1 for GaAs and that of Si is probably due to differences in the material.

In Figure 16 it can be seen that the curves of the implanted and virgin GaAs have the same shape. At low energy density no change in reflectivity or T was observed, but as the energy density was increased there was a rapid rise in the melt time versus energy density curve. After the initial rise in the reflectivity signal (T threshold), the melt time versus energy density curve then goes through two linear increase regions as the energy density increases. In virgin GaAs the curve became somewhat flat from T threshold at about $.21 \text{ J/cm}^2$ to about $.4 \text{ J/cm}^2$. At $.4 \text{ J/cm}^2$ the slope of the melt time

versus energy density curve became much steeper.

The basic shape of the implanted melt time versus energy density curve was established from T for GaAs implanted with 120 keV Te at 10^{14} ions/cm². However, T for GaAs samples implanted with 120 keV Te and Argon (Ar) at 10^{15} ions/cm² and 10^{14} ions/cm² respectively were also measured. Comparing the time-resolved reflectivity measurements on the implanted Te and Ar samples, it appears that the type of implant does not affect the annealing process since both have the same T . Only one GaAs sample implanted with Te at 10^{15} ions/cm² was annealed. The sample was annealed at $.35$ J/cm² and no difference in the melt times of the 10^{15} ions/cm² and the 10^{14} ions/cm² Te implanted samples was observed.

Above $.4$ J/cm² the curve for the implanted samples is the same as that for the virgin within the error of measurements; however, below $.4$ J/cm² the melt time is longer than that of the virgin GaAs. T threshold for the implanted GaAs was determined to be about $.1$ J lower than that of virgin GaAs. To decrease the possibility of error, a virgin sample was first irradiated and then an implanted sample at the same energy density. The difference in T at $.35$ J/cm² for a virgin and implanted sample can be seen in Figures 17 and 18. Three reasons that have been suggested for the differences in T of the implanted and virgin samples below $.4$ J/cm² are: (1) more of the laser energy is absorbed due to the amorphous layer, (2) that the melting temperature of the amorphous layer is less, or (3) that the thermal conductivity of the amorphous layer is less (Ref. 13:20).

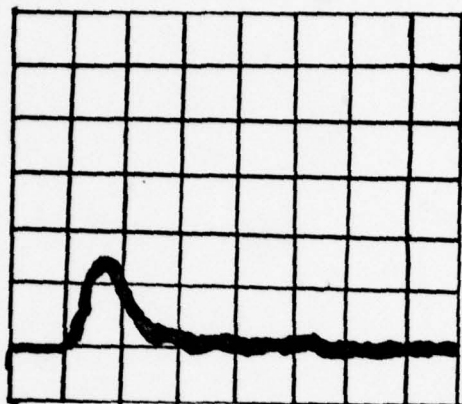


Figure 17. HeNe reflected signal from virgin GaAs annealed with $.35 \text{ J/cm}^2$. Melt time 77 nsec.

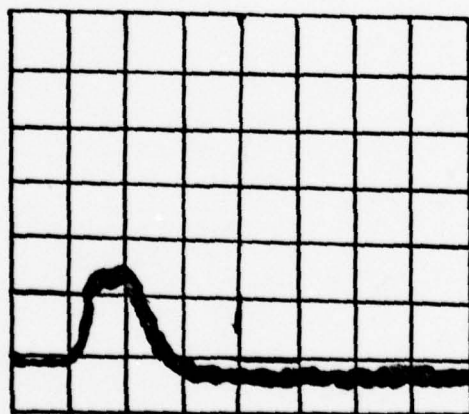


Figure 18. HeNe reflected signal from GaAs implanted with 120 keV Te at 10^{14} ions/cm² annealed with $.35 \text{ J/cm}^2$. Melt time 93nsec.

In Figure 14, numerical solutions for melt depth versus energy density can be seen. Examining the curves for amorphous and virgin Si in Figure 14 shows that a difference in the absorption coefficient will result in a difference in the melting threshold. Therefore, the lower melt threshold observed for the implanted GaAs is expected. Figure 14 also shows the melting threshold for GaAs annealed with a 25 nsec ruby laser pulse to occur at about $.25 \text{ J/cm}^2$ for virgin GaAs which agrees with that found in Figure 16.

The reason that the melt time versus energy curves for the implanted and virgin GaAs become the same at high energy densities is not explainable from the numerical solutions in Figure 14. However, one explanation for why T becomes the same at high energy densities is that once the material has melted both the implanted and virgin material have the same properties. At high energy densities, the melting occurs very early in the laser pulse and so most of the energy is absorbed in the melted material. Therefore, little difference in T should be observed between the implanted and virgin material. As the energy density is decreased, the amount of energy being absorbed in the melted material will decrease and differences in the properties of the material such as the reflectivity and the absorption coefficient will cause more noticeable differences in T.

A good explanation for the differences between Bell Laboratories results and that of this thesis is not available. This is due to the fact that there are several differences in the experiments such as: (1) Bell Laboratories used $\lambda = .53 \mu\text{m}$

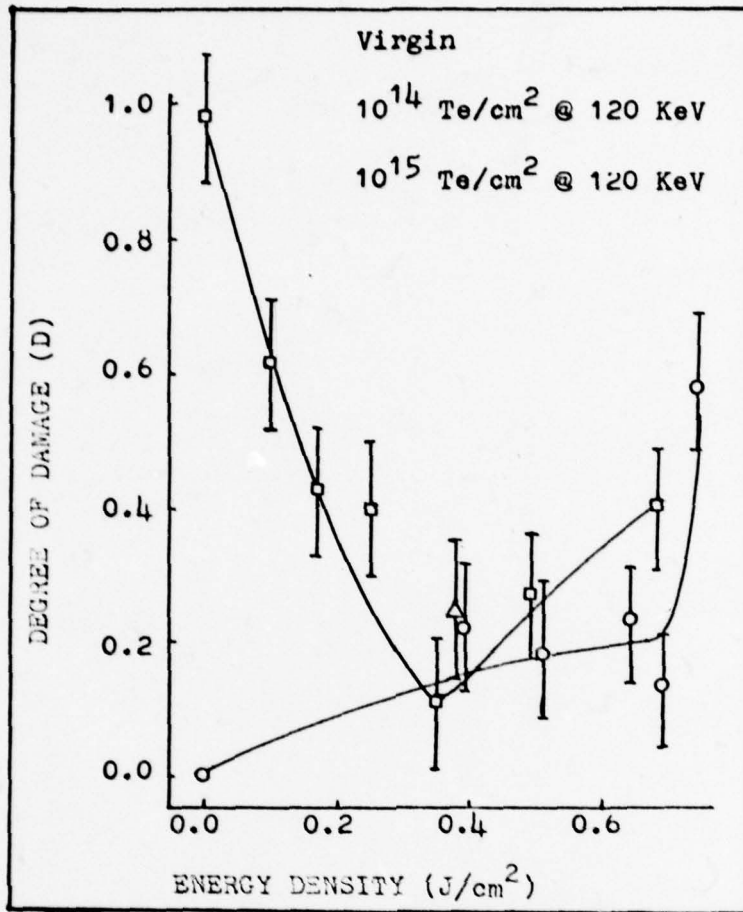


Figure 19. Degree of Damage vs. Laser Annealing Energy Density for GaAs. (Ref. 22)

radiation instead of .69 μm , and (2) the pulse length used by Bell Laboratories was 40 nsec and that for this thesis was 28 nsec. Because Bell Laboratories used .53 μm radiation, the absorption coefficient is larger (Ref. 29:519) and the melt threshold should be lower. However, the pulse length is longer which would tend to cause the melting threshold to increase. Another possible cause is in the measurement of T, because of these differences it is hard to obtain a good explanation for

the differences between the two experiments.

Another method of examining the laser irradiated samples is optical reflectivity techniques (Ref. 22). These results, seen in Figure 19 show the degree of noncrystallinity or damage (D) versus energy density for both the laser irradiated implanted and virgin GaAs. A piece of crystalline material will have a value of D of zero, and an amorphous piece of material will have a D of one (Ref. 22). It can be seen in Figure 19 that D for GaAs implanted with Te at 10^{14} ions/cm² decreases until at $.35$ J/cm² it is as small or smaller than the irradiated virgin. From Figures 17 and 18 it can be seen that the virgin and the implanted GaAs did not have the same T. From Figure 16 it can be seen that the melt time of the implanted sample annealed at $.35$ J/cm² was approximately that of the virgin GaAs at $.4$ J/cm². Evaluation of D above $.35$ J/cm² seems to indicate that the laser irradiation is causing damage to the crystallinity of the sample.

From examination of the samples with a microscope the $.35$ J/cm² annealed implanted sample showed almost no surface damage. As the energy density was increased above $.35$ J/cm² cratering in the surface of the implanted samples became more noticeable. In crystalline GaAs surface damage was not observed until about $.59$ J/cm². Surface damage in the form of scattered craters was reported by Mason (Ref. 5:46) to occur at $.27$ J/cm² in GaAs implanted with Te at 10^{15} ions/cm². The reason for the lower damage threshold could be due to differences in the beam profile.

Using the sheet resistivity measurements in Figure 20 for

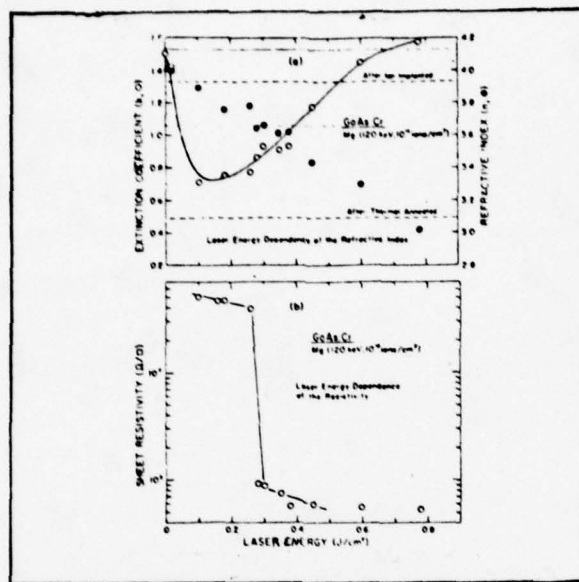


Figure 20. Laser energy dependence of the extinction coefficient and the sheet resistivity. (Ref. 21:601).

CaAs implanted with 120 keV Mg at 10^{15} ions/cm², a large drop in resistivity at about $.28 \text{ J/cm}^2$ can be seen. Comparing the results in Figure 20 with time-resolved reflectivity measurements in Figure 16 place the drop in sheet resistivity at the energy density above the melting threshold. Therefore, there is a large increase in electrically activated impurities due to the melting of the implanted layer of the sample. Also, the initial drop in the extinction coefficient seen in Figure 20 occurring at about $.1 \text{ J/cm}^2$ which is just above the melt threshold. The drop in the extinction coefficient, which is proportional to the absorption coefficient, just above the melt threshold, would indicate that the absorption coefficient decreases at the start of melting. From optical reflectivity techniques, it appears that the energy density required for the lowest extinction coefficient and for the sudden drop in sheet

resistivity in Figure 20 ($.38 \text{ J/cm}^2$) is close to that required for good crystallinity.

Laser Annealing of Si

Both virgin Si and Si implanted with 30 keV In at $10^{15} \text{ ions/cm}^2$ were annealed with the Q-switched ruby laser used to anneal the GaAs. The analysis of the annealing was the same as that of the GaAs.

Results from the time-resolved reflectivity measurement along with those obtained by Bell Laboratories (Ref. 13:17) can be seen in Figure 21. Comparison of the results in Figure 21 with Figure 16 shows similar curves but at about 2.5 times the energy density.

Melting threshold of the implanted Si is about 20% lower than that of the virgin Si but the difference in T decreases until at $.9 \text{ J/cm}^2$ when they are approximately the same. Bell Laboratories, using $\lambda = .53 \mu\text{m}$ found that the difference of melting threshold between virgin and implanted Si to be about 30% (Ref. 13:20). Comparing Bell Laboratories reported values for T versus energy density with the experimental results obtained, it can be seen that Bell Laboratories curve is shifted to lower energy densities. The slopes and general shapes of the melt time versus energy density curves stayed the same. Differences in the data reported by Bell Laboratories and the experimental values obtained along with differences observed between the virgin and implanted Si can be due to differences in the absorption coefficient.

Bell, et.al. (Ref. 33:319) have shown that for Si the

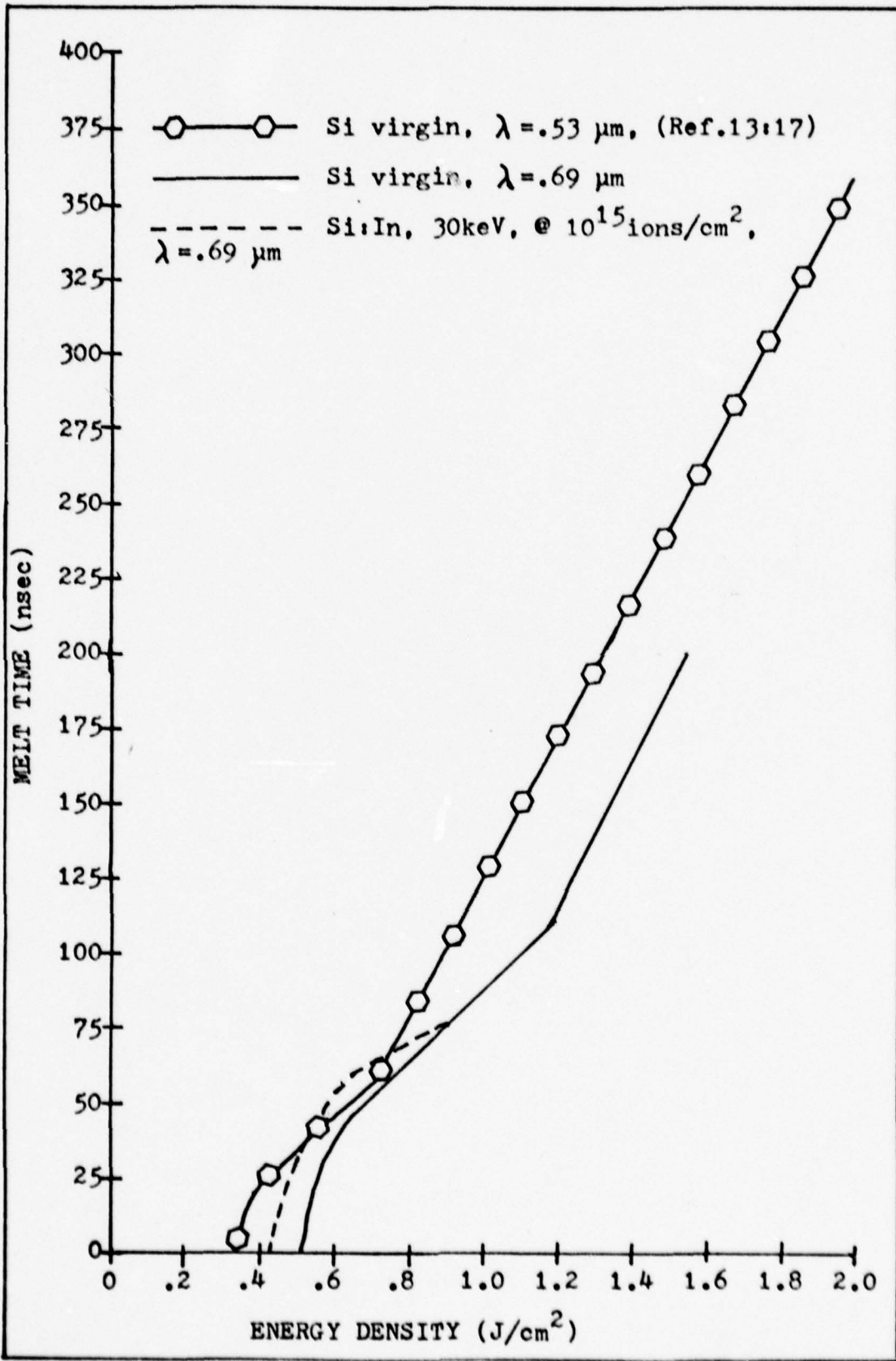


Figure 21. Melt Time of Silicon vs Energy Density

the higher absorption coefficient causes amorphous Si to melt at lower energy densities. These results are shown in Figure 14 and amorphous Si is observed to melt at $.5 \text{ J/cm}^2$ and virgin Si at $.9 \text{ J/cm}^2$. The value for amorphous Si is close to that shown in Figure 21 to be the melt threshold. However, the difference between the implanted and the virgin Si and the melting threshold for the virgin Si do not agree with the results obtained (Ref. 33:319).

The results of the examination of the Si by optical reflectivity can be seen in Figure 22. These results show that no change in crystallinity occurs at $.5 \text{ J/cm}^2$ which corresponds to very little melting having taken place. As the energy density is increased and more melting occurs, the parameter D continues to decrease. No increase in D due to laser induced damage in the crystallinity was observed to about 1.3 J/cm^2 .

From observations with a microscope, there was one crater formed in the center of the annealing at energy densities of $.5 \text{ J/cm}^2$. This crater showed little increase in size from $.95 \text{ J/cm}^2$ to 1.3 J/cm^2 , and non-uniformities in the annealing beam are probably the cause of the crater. Therefore, the experimental set up used to anneal the Si needs to be changed so that the beam profile would be more homogenous.

Using a reflectivity of 33% (Ref. 29:111) for virgin and 45% (Ref. 30:648) for amorphous Si, and the voltage measurements, R_1 was calculated to be 69% and 71% for virgin and amorphous Si respectively. These values are in agreement with the reported value for liquid of 74% (Ref. 31:2111).

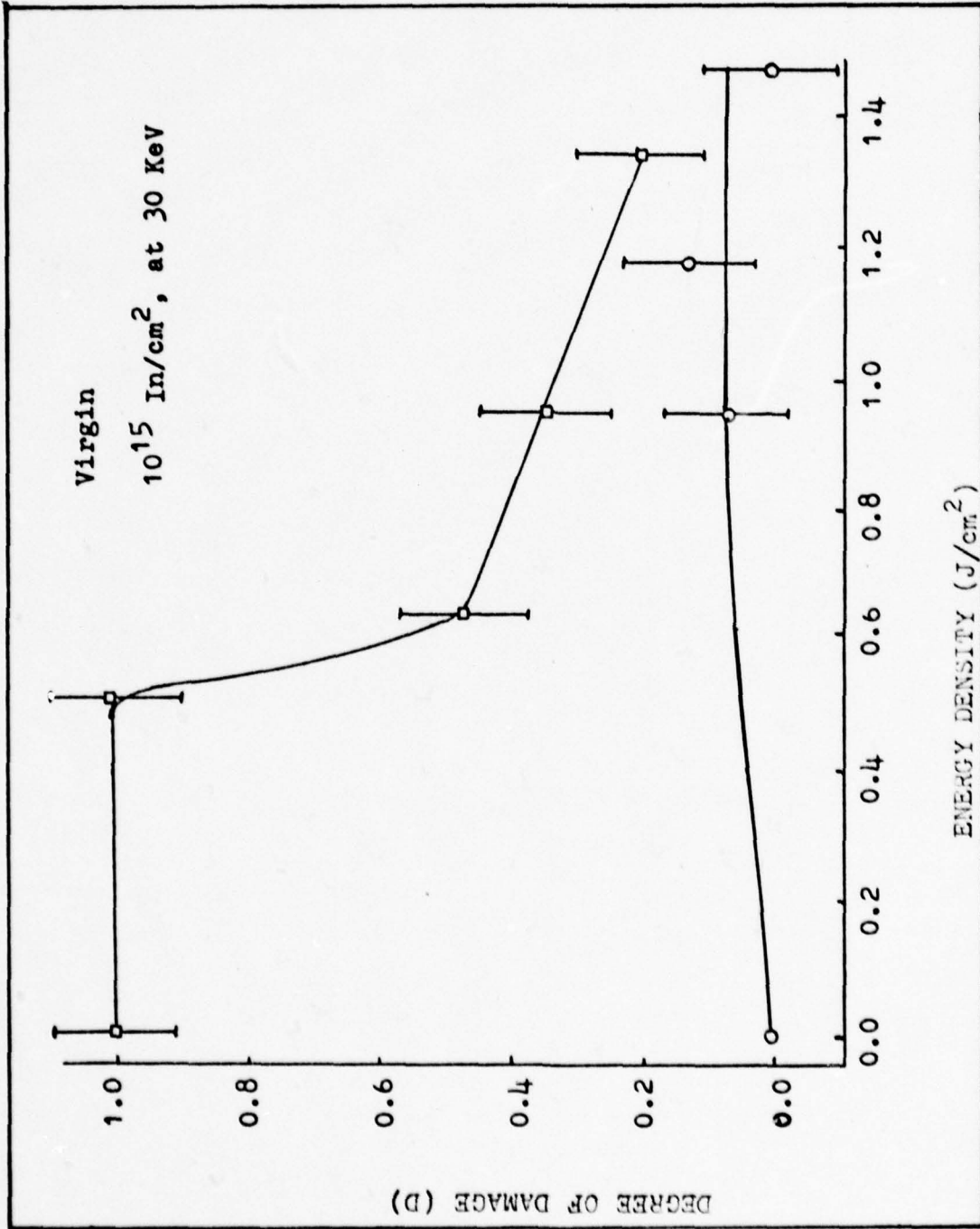


Figure 22. Degree of Damage vs. Laser Annealing Energy Density for Si.
 (Ref. 22)

V. CONCLUSION AND RECOMMENDATIONS

Conclusion

Both virgin and ion implanted Si and GaAs were annealed with a Q-switched ruby laser having a pulse length (T_p) of approximately 28 nsec (FWHM). Examination of the annealed samples was accomplished using time-resolved reflectivity measurements, visual microscopy, and optical reflectivity techniques (Ref. 22). The results obtained were then compared with reported experimental work and numerical calculations.

Using the time-resolved reflectivity measurements, it was determined that the surface of the material did melt above a certain energy density. An exact interpretation of melting is not possible due to lack of information on the reflectivity of Si and GaAs as a function of temperature. The maximum reflected signal (R_1) was calculated to be 59% for GaAs and 69% and 71% for virgin and implanted Si respectively. The value obtained for R_1 of Si is in agreement with the reported value of 74% for liquid Si at 1600°C (Ref. 31:2111).

From the time-resolved measurement, a melt time (T) was defined and plotted against the energy density. The T versus energy density curves were then compared with those obtained by Bell Laboratories. For Si, the curve obtained by Bell Laboratories was shifted to lower energy density values. The shifting to lower energy density is expected due to numerical calculations that have been performed (Ref. 33: 348). These calculation show that amorphous Si will melt before virgin Si due to a higher absorption coefficient. Bell Laboratories

results were obtained using $\lambda = .53 \mu\text{m}$ radiation which does have a higher absorption coefficient in Si than $\lambda = .69 \mu\text{m}$ (Ref. 29:519). Differences between Bell Laboratories results and that of this paper for GaAs are not as easily explained. The difference in the slope of the melt time versus energy density curves result from the way that the melt time (T) was measured.

The time-resolved reflectivity measurements were also used to determine what affect the energy density had on the samples. The results were found to be useful in determining that there is an energy density threshold that must be reached before melting will occur, and that at very high energy densities damage can be detected. The threshold for detecting damage by this technique was found to be much higher than that required to produce scattered craters. Comparing the results with information obtained by optical reflectivity measurements (Ref. 22) revealed that the time-resolved reflectivity measurements by themselves do not give an exact understanding of the degree of anneal.

From optical reflectivity techniques (Ref. 22), it was determined that GaAs is very sensitive to the amount of energy density used in annealing. At too low of an energy density the material was not annealed but at higher energy densities damage to the crystallinity of the surface caused by annealing was observed. Si was not found to be as sensitive to the energy density but an ideal value for the energy density needed to anneal Si was not found. It appeared that the crystallinity of Si would be restored above 1.35 J/cm^2 , which was the maximum

energy density used.

The melt time of samples implanted with Ar was found to be the same as samples implanted with Te. Therefore, the damage to the surface of the sample from ion implantation and not the type of implanted material is believed to cause the lower melting threshold in the implanted material. Only one sample with a different implantation concentration was annealed, and its melt time fell on the melt time versus energy density curve for the implanted GaAs. More samples implanted at different concentration would need to be examined before any conclusions can be reached regarding the effect that the concentration has on the annealing process.

Cratering in Si was observed to occur at energy densities below that required for annealing. These craters were always formed in the center of the sample, and are believed to be caused by non-uniformities in the beam profile. The non-uniformities in the beam profile in Appendix B are not seen; however, from burn patterns taken at low energy densities a hot spot in the center of the burn was observed. The hot spot is small compared with the size of the annealing beam and so it is not detectable in the beam profile measurement.

An effort was made to try and detect whether or not a plasma was formed at the surface of the sample when damage occurred. The method used to detect the plasma was to look for a bright spark. No signs of a plasma were seen even when the surface was completely destroyed.

Recommendations

Because of non-uniformities in the beam profile it is not possible to determine whether cratering is due to the surface of the sample or due to hot spots. By using a single mode laser, different values for the energy density required to produce visual damage might be obtained. Since the center of the beam would probably have the highest energy density, the time-resolved reflectivity measurements taken at the center may be used to detect when damage occurs.

Since there is a possibility that a plasma is formed at the surface of the sample, it would be beneficial to determine whether or not the plasma is formed. Using a Neodymium laser for the first examination may be better because the breakdown threshold is lower for $\lambda = 1.06 \mu\text{m}$.

Time-resolved reflectivity measurements should be taken using $\lambda = .53 \mu\text{m}$ to verify published reports and to examine differences between Bell Laboratories results and that of this thesis. The samples should also be examined with other methods such as optical reflectivity and sheet resistivity to determine the differences that occur because a different wavelength is used. Samples implanted with different concentrations, distribution, and types of impurities can be examined to see what affect the impurities have on the annealing process. To obtain a better idea of what can be determined from the time-resolved reflectivity signal, information on the reflectivity of semi-conducting materials as a function of temperature needs to be obtained.

Examination of the numerical work that has been accomplished

could reveal more information about what occurs during laser annealing. Also, modeling the annealing process on a computer could be useful if information about the thermal and optical properties of both implanted and virgin samples as a function of temperature can be obtained.

BIBLIOGRAPHY

1. Hunter, Lloyd P., Handbook of Semiconductor Electronics, 3rd ed.: 57-59 (1970).
2. Leuchtag, H. Richard, "Laser annealing Shows Promises for Making P-N Junction," Physics Today: 17-19 (July 1978).
3. Robinson, Arthur L., "Laser Annealing : Processing Semiconductors Without a Furnace," Science: 333-335 (July 28, 1978).
4. Krueer, M. R., et. al., Semiconductor Damage (tentative title), Unpublished text, Naval Research Laboratory, Washington, D. C., (1979).
5. Mason, Robert S., "Laser Annealing of Ion Implanted Gallium Arsenide," Masters Thesis, Air Force Institute of Technology Wright-Paterson AFB, Ohio, (1978).
6. Carter, G. and J. S. Colligon, Ion Bombardment of Solids, American Elsevier Publishing Company, Inc.: Chapter 9 (1968).
7. Sze, S. M., Physics of Semiconductor Devices, John Wiley and Sons, (1969).
8. Sittig, Marshall, Doping and Semiconductor Junction Formation, Naves Data Corporation, New Jersey: 273-287 (1970).
9. Khaibullin, I. B., et. al., "Some Features of Laser Annealing" Radiation Effects, Vol. 36, No. 4: 225-233 (1978).
10. Auston, D. H., et. al., "CW Argon Laser Annealing of Ion-Implanted Silicon," Applied Physics Letters, Vol. 33, No. 6: 539-541 (Sept., 1978).
11. Auston, D. H., et. al., "Time-Resolved Reflectivity of Ion-Implanted Silicon During Laser Annealing," Applied Physics Letters, Vol. 33, No. 5: 437-440 (Sept. 1978).
12. Liu, Y. S. and K. L. Wang, "A Transient Optical Reflectivity Study of Laser Annealing of Ion-Implanted Silicon : Threshold and Kinetics," Applied Physics Letters Vol. 34, No. 6: 363-365 (15 March 1979).
13. Auston, D. H., et. al., "Dynamics of Laser Annealing," American Institute of Physics Conference Proceedings, No. 50: 11-26 (1978).

14. Narayan, J., R. T. Young and C. W. White, "A Comparative Study of Laser and Thermal Annealing of Boron-Implanted Silicon," Journal of Applied Physics, Vol. 49: 3912-3917 (1978).
15. Glass, Alexander and Arthur H. Guenther, "A Decade of Damage," Electro-Optical Systems Design: 35-39 (April, 1979).
16. Surko, C. M., et. al., "Calculation of the Dynamics of Surface Melting During Laser Annealing," Applied Physics Letters, Vol. 34, No. 10: 635-637 (15 May 1979).
17. Auston, D. H., et. al., "Dual-Wavelength Laser Annealing," Applied Physics Letters, Vol. 34, No. 9: 558-560 (1 May 1979).
18. Venkatesan, T. N. C., et. al., "Study of Surface Crystallinity and Stoichiometry of Laser-Annealed GaAs Using Time-Resolved Reflectivity and Channeling," Applied Physics Letters, Vol. 35: 88-90 (1 July 1979).
19. Tsu, Raphael, et. al., "Laser-Induced Recrystallization and Damage in GaAs," Applied Physics Letters, Vol. 34, No. 2: 153-155 (15 Jan 1979).
20. Venkatesan, T. N. C., "Dose Dependence in Laser Annealing of Arsenic-Implanted Silicon," Applied Physics Letters, Vol. 33, No. 5: 429-431 (Sept. 1978).
21. Kim, Q., et. al., "Laser Annealing of Ion-Implanted GaAs," American Institute of Physics Conference Proceedings, No. 50: 597-602 (1978).
22. Mullins, Bill W., "Characterization of Laser Annealing of Ion Implanted GaAs and Si Using Optical Reflectivity," Masters Thesis, Air Force Institute of Technology, Wright-Patterson AFB, Ohio, (1979).
23. Tandon, J. L., et. al., "Pulsed-Laser Annealing of Implanted Layers in GaAs," Applied Physics Letters, Vol. 34, No. 9: 597-599 (1 May 1979).
24. Bloemberger, N., "Fundamentals of Laser-Solid Interactions," American Institute of Physics Conference Proceedings, No. 50: 1-9 (1978).
25. Narayan, Jagdish, "Depth of Melting Produced by Pulsed-Laser Irradiation," Applied Physics Letters, Vol. 34, No. 5: 312-315 (1 March 1979).
26. Hofker, W. K., et. al., "Laser Irradiation of Silicon Containing Misfit Dislocations," Applied Physics Letters, Vol. 34, No. 10: 690-692 (15 May 1979).

27. Gat, A., et. al., "Physical and Electrical Properties of Laser-Annealed Ion-Implanted Silicon," Applied Physics Letters, Vol. 32, No. 5: 276-278 (1 March 1978)
28. Smith, J. Lynn, "Surface Damage of GaAs from .694- and 1.06- μ m Laser Radiation," Journal of Applied Physics, 43: 3399 (1972).
29. Willardson, R.K. and Albert C. Beer, Semiconductors and Semimetals, Vol. 3, Academic Press, New York (1966).
30. Seidel, T.E., et.al., "Visible Interference Effects in Silicon Caused by High-Current-High-Dose Implantation," Applied Physics Letters, Vol 29, No. 10: 648 (1976).
31. Shvarev, K.M., et.al., "Optical Properties of Liquid Silicon," Soviet Physics Solid State, Vol. 16, No. 11: 2111-2 (May 1975).
32. Baeri, F., et.al., "Arsenic Diffusion in Silicon Melted by High-Power Nanosecond Laser Pulsing," Applied Physics Letters, Vol. 33, No. 2: 137-40 (15 July 1978).
33. Bell, R.O., et.al., "Calculated Temperature Distribution During Laser Annealing in Silicon and Cadmium Telluride," Applied Physics, Vol. 19: 313-19 (1979).
34. Raizer, Yu P., Laser Induced Discharge Phenomena, Consultants Bureau, New York: 64-76 (1977).
35. Stamm, Michael Richard, "The Formation, Propagation, and Structure of Laser Supported Detonation Waves and Their Effect on Laser-Target Interactions," Ph. D. Thesis, Unpublishes Text, University of Nebraska: (1977).
36. Carslaw, H.S. and J.C. Jaeger, Conduction of Heat in Solids, Clarendon Press, Oxford, (1959).
37. Schultz, J.C. and R.J. Collins, "A Computer Simulation of Laser Annealing Silicon at 1.06 μ m," Applied Physics Letters, Vol. 34, No. 1: 84-7 (1 Jan 1979).
38. Baeri, F., et.al., "A Melting Model for Pulsing-Laser Annealing of Implanted Semiconductors," Journal of Applied Physics, Vol. 50, No. 2: 788-97 (Feb 1979).
39. Wolf, Helmut F., Silicon Semiconductor Data, Vol. 9, Pergamon Press, Oxford (1966).
40. Lukes, F. and E. Schmidt, "The Fine Structure and The Temperature Dependence of the Reflectivity and Optical Constants of Ge, Si, and III-V Compounds," Proceedings of the International Conference on the Physics of Semiconductors. Exeter: 389-94 (1962).

41. Ho, C.Y., et.al., "Thermal Conductivity of the Elements,"
Journal of Physical Chemistry Reference Data 1: 279- 421
(1972).
42. Shaskov, Yu. M., et.al., "Thermal Conductivity of Silicon
in the Solid and Liquid States Near the Melting Point,"
Soviet Physics Solid State, Vol. 8, No. 2: 447-8 (1966).

appears that the energy density required for the lowest extinction coefficient and for the sudden drop in sheet

APPENDIX A

Table I

References to thermal and optical properties of Si and GaAs

| PROPERTY | INFORMATION CONTAINED | MATERIAL | REFERENCE |
|--|--|-------------------------|-----------|
| Absorption Coefficient | function of photon energy ($h\nu$) at 300 °K | virgin GaAs | 29:174 |
| | at 300 °K and 77 °K | virgin GaAs and Si | 7:54 |
| | for 1.06 μm and .69 μm | virgin and amorphous Si | 9:226 |
| Extinction Coefficient and Index of Refraction | for different concentrations of impurities | amorphous GaAs | 21:598 |
| | for different temperature and wavelength | virgin GaAs | 29:518-23 |
| | for liquid Si at 1450 °C and 1600 °C | liquid Si | 31:2111 |
| Mass Density | at 300 °K | virgin GaAs and Si | 7:57 |
| Melting Temperature | | GaAs and Si | 7:58 |
| Reflectivity | function of $h\nu$ | GaAs and Si | 29:111-2 |
| | fine structure from 103 °K to 600 °K | GaAs and Si | 40 |
| | | amorphous Si | 30:648 |
| Specific Heat | at 300 °K | GaAs and Si | 7:58 |
| | from 20 to 10 ³ °K | SI | 39:99 |

Table I continued

| | | | |
|-------------------------|---------------------------------|----------------|--------|
| Thermal Conductivity | as a function of temperature | GaAs and Si | 41 |
| | from 100 to 10^3 °K | GaAs | 39:99 |
| | from 3 to 10^3 °K | Si | 39:99 |
| | at the melting point | Si | 42:447 |

APPENDIX B

Beam Profile

Due to nonhomogeneities in the ruby laser beam, a diffuser and light pipe were used in an effort to make the beam more homogeneous. The light pipe was also used in an effort to get the energy density high enough for annealing.

The problem with using the light pipe was that due to spectral reflections from the inside of the pipe the beam profile was dependant upon the distance from the end of the pipe. From burn patterns it was determined that the beam profile was the most uniform at 4 cm behind the light pipe.

To obtain a rough idea of the distribution of the energy density, the energy transmitted through a 1.4 mm aperture placed 4 cm behind the light pipe was measured. The energy measured was then multiplied by the area of the aperture to obtain an average for the energy density. Due to symmetry in the laser beam, the energy density versus distance from the center of the beam out to 3 mm is shown in Figure 23. At each location four shots were taken and averaged to increase the reliability of the measurements.

Due to the size of the aperture the beam profile in Figure 23 is not completely accurate. Evidence of the inaccuracy is that when Si samples were annealed a crater was formed in the center of the sample. These craters suggest that the energy density in the center is much higher than measured. The size of the hot spot is probably much smaller than the aperture; therefore, it would not be detected in the beam profile measurements.

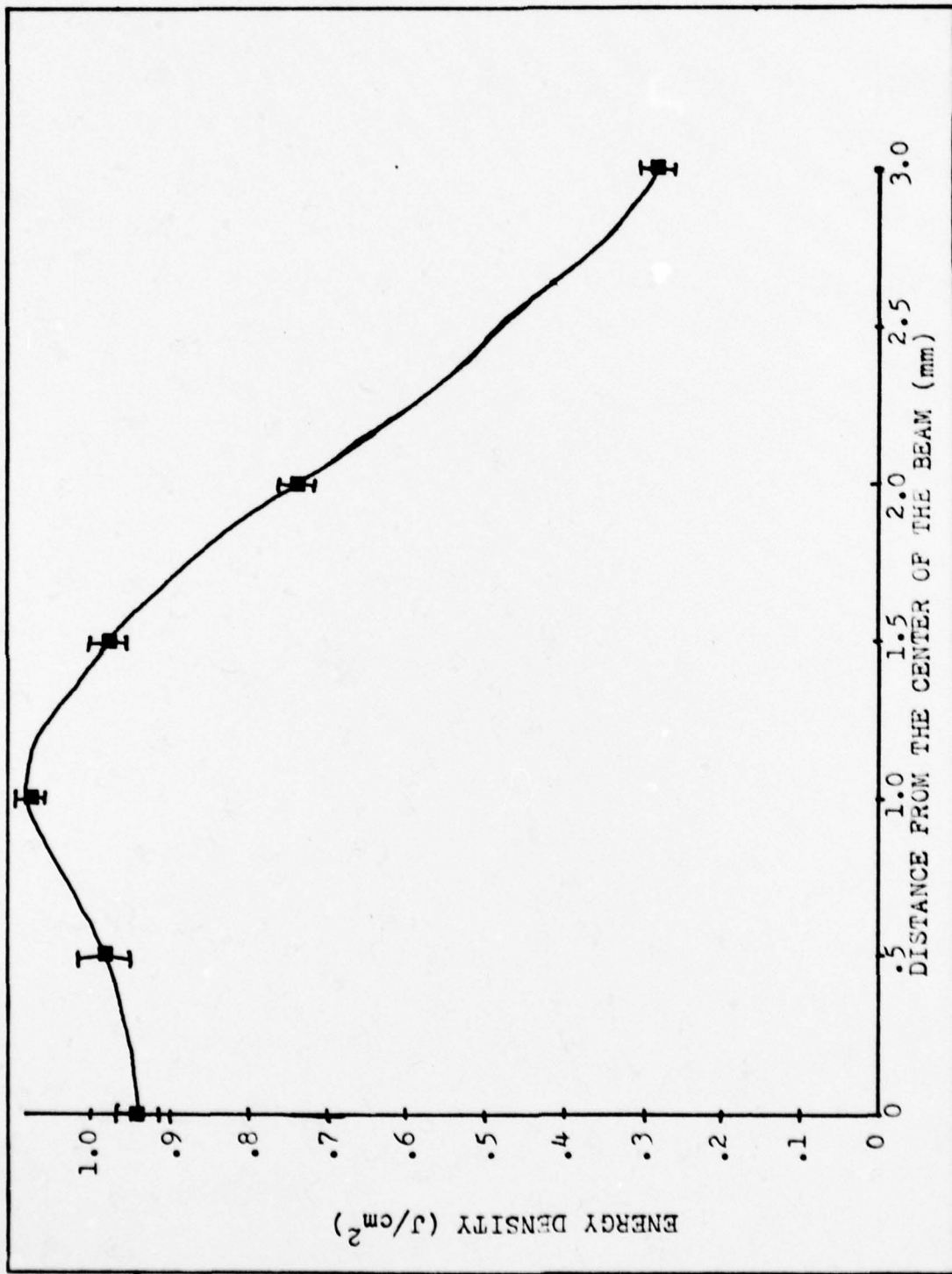


Figure 23. Energy density profile of the annealing beam 4cm behind the end of the light pipe using the 600 lightly frosted diffuser.

VITA

Kenneth Reed Bradley was born on 21 December 1951 in Driggs, Idaho. He was graduated from San Diego State University in May, 1978 with a Bachelor of Science of Physics. He received a commission in the United States Air Force through the ROTC program in June, 1978, and was assigned to the Air Force Institute of Technology at Wright-Patterson Air Force Base later that month.

Permanent Address: 15108 Andorra Way
San Diego, California 92129

UNCLASSIFIED

SECURITY CLASSIFICATION OF THIS PAGE (When Data Entered)

| REPORT DOCUMENTATION PAGE | | READ INSTRUCTIONS BEFORE COMPLETING FORM |
|---|-----------------------|---|
| 1. REPORT NUMBER AFIT/GEP/PH/79D-2 | 2. GOVT ACCESSION NO. | 3. RECIPIENT'S CATALOG NUMBER |
| 4. TITLE (and Subtitle) LASER ANNEALING OF AND LASER INTERACTIONS WITH ION IMPLANT SEMICONDUCTION MATERIALS | | 5. TYPE OF REPORT & PERIOD COVERED MS THESIS |
| | | 6. PERFORMING ORG. REPORT NUMBER |
| 7. AUTHOR(s) KENNETH R. BRADLEY 2Lt USAF | | 8. CONTRACT OR GRANT NUMBER(s) |
| 9. PERFORMING ORGANIZATION NAME AND ADDRESS Air Force Institute of Technology (AFIT-EN) Wright-Patterson AFB, OH 45433 | | 10. PROGRAM ELEMENT, PROJECT, TASK AREA & WORK UNIT NUMBERS |
| 11. CONTROLLING OFFICE NAME AND ADDRESS AF Avionics Laboratory Wright-Patterson AFB, OH 45433 | | 12. REPORT DATE December 1979 |
| | | 13. NUMBER OF PAGES 65 |
| 14. MONITORING AGENCY NAME & ADDRESS (if different from Controlling Office) | | 15. SECURITY CLASS. (of this report) UNCLASSIFIED |
| | | 15a. DECLASSIFICATION/DOWNGRADING SCHEDULE |
| 16. DISTRIBUTION STATEMENT (of this Report) Approved for public release; distribution unlimited. | | |
| 17. DISTRIBUTION STATEMENT (of the abstract entered in Block 20, if different from Report) | | |
| 18. SUPPLEMENTARY NOTES Approved for public release; IAW AFR 190-17 JOSEPH B. HIPPS, Major, USAF Director of Public Affairs | | |
| 19. KEY WORDS (Continue on reverse side if necessary and identify by block number) ANNEALING LASER ANNEALING TIME-RESOLVED REFLECTIVITY | | |
| 20. ABSTRACT (Continue on reverse side if necessary and identify by block number) A Q-switched ruby laser was used to irradiate implanted and unimplanted GaAs and Si. Time-resolved reflectivity measurements, which determine the length of time that the surface of the sample is melted, were performed during the laser annealing process. The length of melt versus energy density was plotted for both the implanted and unimplanted samples. No difference in the melt time was observed between implanted and unimplanted samples at high energy densities. | | |

DD FORM 1473 1 JAN 73 EDITION OF 1 NOV 65 IS OBSOLETE

UNCLASSIFIED

SECURITY CLASSIFICATION OF THIS PAGE (When Data Entered)

UNCLASSIFIED

SECURITY CLASSIFICATION OF THIS PAGE(When Data Entered)

(Block 20 continued)

The threshold for melting in the implanted samples was found to be lower than the virgin samples, and the energy density required to produce melting in GaAs was about $2/5$ that needed for Si.

The results obtained were compared to reported experimental work and numerical calculation on laser annealing. Optical reflectivity techniques, performed by Lt. Mullins were used to determine the crystallinity of the samples after annealing.

UNCLASSIFIED

SECURITY CLASSIFICATION OF THIS PAGE(When Data Entered)